การศึกษาและเปรียบเทียบอัตราการย่อยสลายฟีนอลในน้ำด้วยตัวเร่ง ในเครื่องปฏิกรณ์ฟลูอิไดซ์เบดแบบสามเฟส

นางสาวมาลิน มุ่งมาตร

วิทยานิพนธ์นี้เป็นส่วนหนึ่งของการศึกษาตามหลักสูตรปริญญาวิศวกรรมศาสตรมหาบัณฑิต
สาขาวิชาวิศวกรรมเคมี ภาควิชาวิศวกรรมเคมี
คณะวิศวกรรมศาสตร์ จุฬาลงกรณ์มหาวิทยาลัย
ปีการศึกษา 2549

ISBN 974-14-3005-1

INVESTIGATION AND COMPARISON OF CATALYTIC DECOMPOSITION RATES OF AQUEOUS PHENOL IN THREE-PHASE FLUIDIZED BED REACTOR

Miss Malin Mungmart

A Thesis Submitted in Partial Fulfillment of the Requirements
for the Degree of Master of Engineering Program in Chemical Engineering
Department of Chemical Engineering
Faculty of Engineering
Chulalongkorn University
Academic year 2006

ISBN 974-14-3005-1

Thesis Title	INVESTIGATION AND COMPARISON OF CATALYTIC DECOMPOSITION RATES OF AQUEOUS PHENOL IN THREE-PHASE FLUIDIZED BED REACTOR
By	Miss Malin Mungmart
Field of Study	Chemical Engineering
Thesis Advisor	Associate Professor Tawatchai Charinpanitkul, D.Eng.
Thesis Co-Advisor	Professor Wiwut Tanthapanichakoon, Ph.D.

Accepted by the Faculty of Engineering, Chulalongkorn University in Partial Fulfillment of the Requirements for the Master's Degree

..... Dean of the Faculty of Engineering
(Professor Direk Lavansiri, Ph.D.)

THESIS COMMITTEE

..... Chairman
(Assistant Professor Seeroong Prichanont, Ph.D.)

..... Thesis Advisor
(Associate Professor Tawatchai Charinpanitkul, D.Eng.)

..... Thesis Co-Advisor
(Professor Wiwut Tanthapanichakoon, Ph.D.)

..... Member
(Assistant Professor Joongjai Panpranot, Ph.D.)

..... Member
(Apinan Soottitantawat, D.Eng)

มาลิน มุ่งมาตร : การศึกษาและเปรียบเทียบอัตราการย่อยสลายฟีนอลในน้ำด้วยตัวเร่งโดยเครื่องปฏิกรณ์ฟลูอิไดซ์เบดแบบสามเฟส (INVESTIGATION AND COMPARISON OF CATALYTIC DECOMPOSITION RATES OF AQUEOUS PHENOL IN THREE-PHASE FLUIDIZED BED REACTOR) อ. ที่ปรึกษา : รศ.ดร. ธวัชชัย ชรินพาณิชกุล, อ. ที่ปรึกษาร่วม : ศ.ดร. วิวัฒน์ ตัณฑะพานิชกุล, 76 หน้า, ISBN 974-14-3005-1

ในงานวิทยานิพนธ์นี้ ได้ทำการศึกษาการสลายตัวของสารละลายฟีนอลเจือจางโดยใช้เครื่องปฏิกรณ์แบบฟลูอิไดซ์เบดสามวัฏภาค ที่มีปริมาตรรวมเชิงประสิทธิผล 235 มิลลิลิตร แล้วทำการเปรียบเทียบอัตราการสลายตัวโดยใช้โอโซนเพียงอย่างเดียว ตัวเร่งปฏิกิริยาไททาเนียมไดออกไซด์บนเม็ดซิลิกา ตัวเร่งปฏิกิริยาโลหะ (นิกเกิล หรือ โคบอลท์) ที่ถูกตรึงอยู่บนเม็ดคาร์บอนที่มีรูพรุนระดับเมโซพอร์ และ โอโซนร่วมกับตัวเร่งปฏิกิริยาที่กล่าวมาอย่างใดอย่างหนึ่ง ในการนี้ได้กำหนดอัตราการไหลของก๊าซ และของเหลวให้คงที่เท่ากับ 1 ลิตร/นาที และปริมาณตัวเร่งปฏิกิริยาเท่ากับ 5 กรัมต่อกะ จากผลการทดลองในการกำจัดสารละลายฟีนอลความเข้มข้น 10 มิลลิกรัมต่อลิตร ปริมาตร 2 ลิตร พบว่า การใช้ตัวเร่งปฏิกิริยาไททาเนียมไดออกไซด์โดยปราศจากโอโซนนั้นจะให้ผลต่ำที่สุด (ค่าคงที่ของปฏิกิริยาในช่วงแรกเริ่ม k เท่ากับ 0.0066 ต่อนาที) อย่างไรก็ตาม เมื่อใช้ตัวเร่งปฏิกิริยาไททาเนียมไดออกไซด์ร่วมกับโอโซนที่ผลิตจากอากาศ จะให้ผลที่ดีขึ้น (ค่า k เท่ากับ 0.0492 ต่อนาที) กรณีที่ใช้โอโซนเพียงอย่างเดียวในการบำบัด ประสิทธิภาพในการบำบัดของโอโซนที่ผลิตจากก๊าซออกซิเจนบริสุทธิ์ (ค่า k เท่ากับ 0.1263 ต่อนาที) มีค่าสูงกว่าโอโซนที่ผลิตจากอากาศ (ค่า k เท่ากับ 0.0236 ต่อนาที) ส่วนในกรณีที่ใช้ตัวเร่งปฏิกิริยาโลหะร่วมกับโอโซนที่ผลิตจากอากาศ ตัวเร่งปฏิกิริยาโลหะโคบอลต์ (ค่า k เท่ากับ 0.1944 ต่อนาที) มีประสิทธิภาพสูงกว่าตัวเร่งปฏิกิริยาโลหะนิเกิล (ค่า k เท่ากับ 0.1713 ต่อนาที) นอกจากนั้น เมื่อใช้ตัวเร่งปฏิกิริยาโลหะนิเกิลร่วมกับโอโซนที่ผลิตจากก๊าซออกซิเจนบริสุทธิ์ จะให้ผลการกำจัดฟีนอลได้ดีขึ้น โดยค่าคงที่ของปฏิกิริยา k จะเพิ่มขึ้นจาก 0.1713 เป็น 0.2158 ต่อนาที และฟีนอลสามารถถูกย่อยสลายสมบูรณ์ภายใน 10 นาที จากผลดังกล่าว คาดว่าในกรณีที่ใช้ตัวเร่งปฏิกิริยาโลหะโคบอลต์ร่วมกับโอโซนที่ผลิตจากก๊าซออกซิเจนบริสุทธิ์น่าจะให้ค่า k เพิ่มขึ้นในระดับเดียวกัน ผลิตภัณฑ์ขั้นกลางที่เกิดขึ้นระหว่างปฏิกิริยาการสลายตัวของฟีนอล เช่น ไฮโดรควิโนนและคาทิชอลนั้น พบว่า จะถูกย่อยสลายต่อไปจนคงเหลือความเข้มข้นต่ำมาก

ภาควิชา.....วิศวกรรมเคมี.....	ลายมือชื่อนิสิต.....มาลิน มุ่งมาตร.....
สาขาวิชา...วิศวกรรมเคมี.....	ลายมือชื่ออาจารย์ที่ปรึกษา.....
ปีการศึกษา.....2549.....	ลายมือชื่ออาจารย์ที่ปรึกษาร่วม.....

##4770412121: MAJOR CHEMICAL ENGINEERING
KEY WORD: PHENOL/ THREE PHASE FLUIDIZED BED/ PHOTOCATALYST/ METALLIC CATALYST/ MESOPOROUS SUBSTRATE

MALIN MUNGMART: INVESTIGATION AND COMPARISON OF CATALYTIC DECOMPOSITION RATES OF AQUEOUS PHENOL IN THREE-PHASE FLUIDIZED BED REACTOR. THESIS ADVISOR: ASSOCIATE PROFESSOR TAWATCHAI CHARINPANITKUL, D.Eng. THESISCO-ADVISOR: PROFESSOR WIWUT TANTHAPANICHAKOON, Ph.D., 76 pp. ISBN 974-14-3005-1

A batch three-phase fluidized-bed reactor (TPFBR) with an effective total volume of 235 mL was used to investigate the decomposition of dilute aqueous phenol. Comparison of the phenol decomposition rates under different conditions: employing only ozone (O_3), only TiO_2 photocatalyst on silica beads, only metal catalyst (Ni or Co) on mesoporous carbon beads, and ozone together with one of the mentioned catalysts, were carried out. The gas and liquid flow rate were kept constant at 1 L/min and the catalyst loading was 5 g per batch. The experimental results in the decomposition of 2 L of 10 ppm phenol solution revealed that using TiO_2 without ozone gave the worst result (initial reaction rate constant k = 0.0066 min^{-1}). However, when combined with ozone that generated from air, the result was better (k = 0.0492 min^{-1}). In the case of using only ozone for decomposition, the efficiency of ozone generated from pure oxygen (k = 0.1263 min^{-1}) was higher than that generated from air (k = 0.0236 min^{-1}). Meanwhile in the case of using metallic catalyst with ozone generated from air, Co-metallic catalyst (k = 0.1944 min^{-1}) had higher efficiency than Ni-metallic catalyst (k = 0.1713 min^{-1}). Using Ni-metallic catalyst with ozone generated from pure oxygen could provide the even better result. The rate constant would increase from 0.1713 to 0.2158 min^{-1} and complete degradation of phenol can be essentially achieved within 10 min. It was expected that using Co-metallic catalyst with ozone generated from pure oxygen should enhance the rate constant at a similar level. Some intermediate products such as hydroquinone (HQ) and catechol (CC) were also detected but they were eventually decomposed down to very low concentrations.

Department.....Chemical Engineering.....	Student's signature Malin Mungmart
Field of Study.....Chemical Engineering....	Advisor's signature T. Charinpanitkul
Academic Year.....2006.....	Co-advisor's signature W. Tanthapanichakoon

ACKNOWLEDGEMENTS

The author would like to express her greatest gratitude to her advisor, Assoc. Prof. Dr. Tawatchai Charinpanitkul and co-advisor Prof. Dr. Wiwut Tanthapanichakoon, for their invaluable guidance throughout this study. In addition, I would also grateful to thank to Asst. Prof. Dr. Seeroong Prichanont Seeroong Prichanon, as the chairman, Asst. Prof. Dr. Joongjai Panpranot, and Dr. Apinan Soottitantawat, as members of the thesis committee for their kind advices.

Many thank for kind suggestions and useful help, in particular all catalysts used in this study, should be addressed to Dr. Takuji Yamamoto of AIST Japan and Mr. Apiluck Eiad-ua. Moreover, the author would like to acknowledge the Center of Excellence on Catalysis and Catalytic Reaction Engineering for supporting the analytical test and instruments such as XRD and H_2 chemisorption and Mr. Piyawat Supphasrirongjaroen for his hospitality to analyze the sample.

Furthermore, many thanks should be acknowledged to Mr. Poonlasak Muthakarn and her friends in Center of Excellence in Particle Technology (CEPT) Laboratory of Chulalongkorn University who always provide co-operation along her thesis study.

Finally, she also would like to dedicate this thesis to her parents who have always been the source of her support and encouragement.

CONTENTS

Page

LIST OF TABLES

LIST OF FIGURES

LIST OF FIGURES (cont.)

Figure **Page**

LIST OF FIGURES (cont.)

Figure **Page**

CHAPTER I

INTRODUCTION

1.1 Background

Situation of contamination due to organic compounds in public reservoirs of Thailand has become a crucial issue related directly to industrial development. Among those contamination, phenol and its derivatives are violently present in wastewaters emitted by many industries such as wood preservative, pesticide, textile, paper and dye industrial. There are essential requirements of efficient treatment system, which could meet legally regulated standard and economic constraints.

In general, there are a lot of processes proposed to treat the wastewater. However, it is well known that phenolic compounds can resist effective removal using conventional methods which are biological decomposition or adsorption by activated carbon. Therefore, catalytic oxidation system is proposed as a promising alternative because of its various advantages such as non-toxicity, high stability and high activity for decomposing those pollutants.

Photo-catalysts have been used for a purpose of pollutant decomposition by high activated reactions of waste materials, pollutants, and harmful bacteria. Meanwhile metallic catalyst produced by a novel technology is also interesting. The metallic catalyst can react and decompose the phenolic compounds without light irradiation while the photocatalyst oppositely needs light for stimulating the reaction. In practice, photo catalysis systems are preferably expected to use sun light as a light source. However, because the sunlight intensity strongly depends on the weather conditions, leading to consistent energy which is not enough for treating the stable compounds of complex structure. Therefore a high power with short wavelength like UV-lamps has been used instead. These requirements for photocatalytic decomposition system result in higher operating cost including catalyst regenerating cost and electricity cost for irradiation. By this reason, the metallic catalyst seems to be more interesting. Especially when a super oxidizing agent which is ozone is incorporated in such the system it will potentially help increasing decomposition performance.

Meanwhile, three-phase reactors, which could provide intimate contact among gases, liquid, and solid phases, have gained increasing attention in a wide range of industrial applications. These reactors have various merits of simplicity in construction and operation, low operating cost and flexibility for liquid and solid phase residence times. Furthermore advantages of three-phase reactors are as follows;

(1) Intense contact between the phases.

(2) High degree of mixing resulting in isothermal operation.

(3) High values of effective interfacial area and overall mass transfer coefficient.

(4) Large heat capacity of the liquid phase and high heat transfer coefficients providing advantageous in temperature control.

(5) Catalyst can be continuously added and withdrawn without any erosion or plugging problems.

(6) Cushioning effect of the liquid leading to less particle abrasion.

Due to these advantages, three-phase fluidized bed reactors have been widely used, for example, coal conversion process, catalytic hydrogenation, and hydro-desulfurization of residual oil. The current applications for wastewater treatment and biochemical processes are also commonly encountered [1].

In this research the efficiency of metallic catalyst (nickel or cobalt) on mesoporous carbon bead produced by sol-gel method was investigated and compared with a commercial TiO_2 photocatalyst on silica beads in a lab scale three-phase fluidized bed reactor. Ozone was selected as an oxidizing gas to be carried by ambient air fed from a compressor. The effect when combining with each catalyst was studied. Finally the possibility for degrading phenol solution in a large volume was tested by using pilot scale 3-phase fluidized bed reactor.

1.2 Objective

The objective of this research is to investigate and compare a decomposition rate of aqueous phenol by using a lab-scale fluidized bed reactor with catalyst immobilized on mesoporous support (catalytic oxidation and photocatalytic decomposition reaction) and / or ozone (ozonation reaction).

1.3 Scope

1. Design and set up lab-scale wastewater treatment system.
   - Reactor: Fluidized bed reactor
   - Catalyst: Metal and photo catalyst on mesoporous beads
   - Oxidizing agent (oxidant): Ozone (O_3)

2. Test the catalytic decomposition of phenol.
   - Range of catalyst loading is 1-20 g.
   - Range of phenol concentration is 10-100 ppm.
   - The solution flow rate is 1 L/min.
   - Gas flow rate is 1 L/min

3. Analyze the decomposition of phenol and intermediate product by
   - HPLC (High performance liquid chromatography, Shimadzu column class VP)
   - TOC (Total organic carbon analyzer, Shimadzu TOC-VCPH)

4. Analyze the characteristic of catalyst by
   - XRD (X-ray diffraction, SIEMENS D5000)
   - H_2 chemisorption (Micromeritics ChemiSorb 2750)
   - N2 physisorption (BEL Japan Inc., BelSorp 2)

CHAPTER II

LITERATURE REVIEW

T. Keiichi et al., (1996) [2] studied about the photocatalytic of water treatment on immobilized TiO_2 combined with ozonation. The intermediate organic acids form during the degradation of phenol disappeared rapidly with the incorporation of photocatalyst. Pretreatment by O_3 leads to the formation of hydrophilic compounds as intermediates, which are more degradable by UV/TiO_2 than by O_3. The photocatalytic process is slow and can only be used for solution of low concentration. The photocatalytic method combined with ozonation provides rapid degradation.

A.J.Feitz et al., (2000) [3] evaluated two large pilot scale fixed bed photo catalytic reactors. One was packed-bed reactor with 140 $mg.m^{-2}.h^{-1}$ and the other was coated-mesh reactor with 20 $mg.m^{-2}.h^{-1}$. They used TiO_2 as a catalyst to remove 2 mg/L phenol solution and 100 mg/L dichloroacetic acid solution. The coated-mesh reactor had lower degree of removal attributed to insufficient surface contact times and low level of available attached TiO_2. It was found that the packed-bed reactor removed 100 $mg.l^{-1}$ dichloroacetic acid only 40% lower than ideal suspension system.

M.F.J. Dijkstra et al., (2001) [4] compared photocatalytic degradation between suspended system (slurry reactor SR), immobilized systems with coated wall as a thin film (tubular reactor TR), and packed by glass beads (packed bed reactor PBR) which had no need of separation step of the catalyst after purification. Degussa P-25 TiO_2 was used as a photocatalyst to degrade formic acid. In PBR, there was no mass transfer limited occurring and rate of reaction was pseudo-zero order kinetics. So, PBR could provide degradation rate faster than that of TR. In addition, it was found that the light intensity in PBR will decrease rapidly over the first layer of glass beads.

J.H. Lee et al., (2003) [1] enhanced the methyl orange destroying performance of fluidized reactors in photocatalytic system. One was the TiO_2 film, exhibited in anatase phase with particle size around 50 nm, attached on UV-lamp by dip-coating method. The other was the 0.1 wt% TiO_2 powder added to the reactant solution. They prepared the catalyst film and powder from TiO_2 colloidal solution which obtained by

sol-gel method. For TiO_2 film photo system, the conversion reached 100% after 4 h in air bubbling of 500 ml/min while in 0.1 g/l TiO_2 powder photo system used 5 h. It was concluded that the film photo system was more useful than the powder photo system.

L. Zhang et al., (2003) [5] developed a tubular photocatalytic reactor using ceramic cylindrical tube coated with Pt-loaded TiO_2 film and UV lamp for water purification. The water was circulated through the reactor via a buffer reservoir for aeration. The oxygen molecules from aeration would prohibit the recombination of excited electron (e^-) and positive hold (h^+) and make the $OH^\bullet$ radical came more. Therefore, with the aeration, the oxidization of chemical compounds was higher and the decomposition rate was faster.

K. Nakano et al., (2004) [6] studied photocatalytic degradation of Dinitrophenol (DNP) on commercial TiO_2/SiO_2 catalyst. More than 90 % of aromatic compound decomposed to carbon dioxide completely in 100 min. By pilot scale fixed bed flow reactor, city water was treated under the sunlight. Found that total organic carbon (TOC) and double boned organic compounds were degraded. However, the catalyst needed to regeneration by washing with acid solution (ex. hydrochloric acid, nitric acid or sulfuric acid) for 1 week because the agglomeration of red iron made it fouled.

A.A.C. Magalhes et al., (2004) [7] prepared porous TiO_2 in form of anatase in field of wastewater by sol-gel method using solutions of tetra isopropylorthotitanate containing polyethylene glycol (PEG) with different molecular weight (2000 and 3400) in order to detected an effect on the structure of titania and its photo-catalytic activity in degradation of phenol. Gel sample were dried at 100 $^\circ$C then thermally treated at 520 $^\circ$C. At temperature above 500°C, the crystallization of TiO_2 occurred in anatase phase and transformed to rutile phase at above 600 $^\circ$C. PEG improved the specific area, pore volume, and anatase dispersion. Therefore, the photo-catalytic of TiO_2 would be greater with the addition of PEG. It was observed that the greatest photo-catalytic activity material was the sample with 2.0 g PEG 2000.

C.M. Ling et al., (2004) [8] studied the performance of photo-catalytic reactors using immobilized TiO_2 film on glass tube by sol-gel method (1 Titanium isopropoxide: 8 isopropanol: 3 acetyl acetone: 1.1 H_2O: 0.05 acetic acid; in molar

ratio). SEM, XRD and EDX analysis were used to characterize the synthesized TiO_2 thin film. They tested the reactors in 2 different modes, a) tubular photo-catalytic reactor with re-circulation mode and b) batch photo-catalytic reactor, to study the effects of initial concentration (phenol and methylene blue dye), H_2O_2, air bubbling, stirring speed, pH and light intensity. The $t_{1/2}$ half-life time, of photo-catalytic degradation of phenol was 56 min at the initial concentration of 1000 μM in the batch reactor. In tubular reactor, 5 re-circulation passes with resident time of 2.2 min (single pass) could degrade 50% of 40 μM methylene blue dye. In addition, TiO_2 film was equally active as TiO_2 powder catalyst.

T. Kanki et al., (2005) [9] developed TiO_2-coated spherical ceramic particles and applied to two types of test-scale fluidized bed reactors. Two light sources were applied to the system as inside the reactor (254 nm) and outside reactor (356 nm) for water purification. They used phenol and bisphenol A as contaminants. With the configuration a), 10 mg/L of phenol and bisphenol A in 2L water could be decomposed in about 200 min and be mineralized in 300 min. While the configuration b) required 20 h to mineralize10 mg/L in 1L water.

M. Kouichi et al., (2006) [10] developed a novel Ni/carbon catalyst and used to gasify organic compounds dissolved in the wastewater with TOC concentration from 0.2 to 2% for producing CH_4 and H_2. The results showed that up to 99% carbon conversion can be achieved at 360 ºC, and 20 MPa. A conversion mechanism was consists of decomposition of big molecules to small molecules on the metal surface and steam gasification of small molecules to produce CO and H_2 (followed by CO methanation and CO shift reaction). Catalyst was found to be highly active and stable and no sintering was observed even after 100 h of reaction time.

CHAPTER III

PHENOL AND DEGRADATION REACTION

3.1 Phenol

Phenol is a colorless-to-white solid when pure and has a distinct odor that is sickeningly sweet and tarry. The molecular formula of phenol is C_6H_5OH (see the molecular structure in **Figure 3.1**).

Figure 3.1 Molecular structure of phenol

Phenol evaporated more slowly than water and moderated amount can form a solution with water in addition it can catch on fire. Phenol and its derivatives are violently present in many industrial wastewaters such as wood preservative, pesticide, textile, paper and dye industrial. The largest single use of phenol is as an intermediate in the production of phenolic resins, caprolactam (which is used in the manufacture of nylon 6 and other synthesis fibers) and bisphenol A (which is used in the manufacture of epoxy and other resins). Phenol is also used as a slimicide (a chemical toxic to bacteria and fungi characteristic of aqueous slimes), as a disinfectant, and in medicinal preparations.

Exposure to phenol may take place at work place or home. Phenol is present in a number of consumer products. These include ointments, ear and nose drops, mouthwashes and antiseptic lotions. For persons not exposed to phenol in the workplace, possible routes of exposure include breathing industrially contaminated air, inhaling cigarette, drinking water from contaminated surface water or ground supplied, skin contact or swallow products containing phenol. This type of exposure is expected to occur infrequently and generally occur over a short time period.

The short term effects from breathing are respiratory irritation, headaches and burning eyes. Chronic effects of high exposure included weakness, muscle pain, anorexia and weight loss while the effects of chronic low level exposures included increases in respiratory cancer, heart disease and effects on immune system. Ingestion of very high concentrations of phenol has resulted in death. Effects reported in dermal exposure to phenol include liver damage, diarrhea, dark urine and red blood cell destruction. Phenol can have beneficial effects when used for medicals reasons. It is an antiseptic (kill germ) or an anesthetic (relieve pain). It destroys the outer layers of skin to remove warts and to treat other skin blemishes and disorders.

The acceptable phenolic compound concentration to be treated in central wastewater treatment process must be controlled at the industrial effluent standard (1.0 mg/l). This means that any particular plant (located in the industrial estates) which discharges phenolic and related compounds greater than the Industrial Estate Authority of Thailand (IEAT) acceptable limits (1.0 mg/l for phenolic compounds) must have their own effective wastewater treatment unit before transferring the wastes to the central treatment process.

3.2 Degradation methods

For the past few decades, there have been many ways for removal of phenol from flow effluents such as biological and chemical oxidation, adsorption on granular activated carbon, chlorination and ozonation.

In biological system, pH and temperature control are necessary and a large land space is required while in chemical system, hydrogen peroxide and potassium permanganate, this method is more expensive and appear to be a reasonable method of phenol treatment for smaller flows. For carbon adsorption, phenol in the final effluent is produced in the low level but the cost of this method included the carbon contact vessel, carbon regenerated system and an associated apparatus is expensive. With chlorination, there are several shortcomings such as the sophistication of correct chlorine dosage, the need of pH control and the generated more toxic chlorophenols. Meanwhile in ozonation, it should be cautioned that ozone may be irritating or toxic depending upon exposure. Direct extended contact with ozone should be avoided [12].

The treatment of many industrial waste stream by traditional non-catalytic chemical process may be too energy intensive with adaptable catalyst, energy consumption of various oxidation procedure may be decreased [13]. Nowadays an advance oxidation process using a metal oxide catalysts for decomposing the phenolic compounds are developed for the use of wastewater treatment system. In this research the removal of phenol is investigated under the ozonation, catalytic oxidation, photo catalytic oxidation and the ozonation combined with one of them.

3.2.1 Catalytic oxidation

Different methods for treating industrial waste water containing organic pollutants have been widely reported. The choice of treatment depends on the level of phenol concentration, on economics and easy control, reliability and treatment efficiency. Oxidation of dilute aqueous solutions of refractory pollutants by using oxygen over a solid catalyst offers an alternative to the techniques (for example, noncatalytic wet-air oxidation, biological oxidation, oxidation in supercritical water, and physical adsorption) as a means of purifying waste waters.

The key issue in the process of effective oxidation of phenolics in water is the catalyst which must have high mechanical strength, chemical stability, and hydrophobicity; actively participate in the oxidation reactions; to be stable in water and facilitate the complete oxidation of the phenolics to carbon dioxide. Transition-metal oxides have proved to be active in the catalytic reactions of complete degradation of phenol and its derivatives in waste waters [14].

Metal oxides can be classified according their physico-chemical properties. One of these properties is the stability of metal oxide. Metals with unstable high oxidation state oxides, such as Pt, Pd, Ru, Au, and Ag do not perform stable bulk oxides at moderate temperatures. Most of the commonly used metal oxide catalysts (Ti, V, Cr, Mn, Zn, and Al) have stable high oxidation state oxides. Fe, Co, Ni, and Pb belong to group with intermediate stability of high oxidation state oxides. It is a well-known fact that metal oxides are usually less active catalysts than noble metals. Nevertheless, to majority of applications metal oxides are more suitable since they are more resistant to poisoning. In addition, combining two or more metal oxide catalysts may improve non-selectivity and catalytic activity [13].

3.2.1.1 *Mechanism of catalytic oxidation [15]*

The mechanism of the oxidation of phenols is extremely complex and is not yet fully understood. It is generally accepted that the oxidation of phenol by molecular oxygen is basically an electrophillic reaction and the rate limiting step is the reaction between the aryloxy radical with oxygen [16]. In accordance with the proposed scheme (see **Figure 3.2**), the oxidation process starts with the adsorption of the substrate (PhOH) on the catalyst surface and the simultaneous tearing off of an H-atom from the phenolic OH^-group, which combines with the active oxygen (O−) of the catalyst to form surface $OH^{\bullet}$. The chemisorbed phenol forms a complex I_1 with the reduced form of the catalyst cation ($Me.^{(n-1)+}$). The latter passes consecutively via a series of surface complexes (I_2–I_4) with a different degree of oxidability, which possess probably the following nature respectively: I_2 —phenoxyradical type, similar to I_1; I_3 — carboxilate complex, while I_4 has a carbonate character.

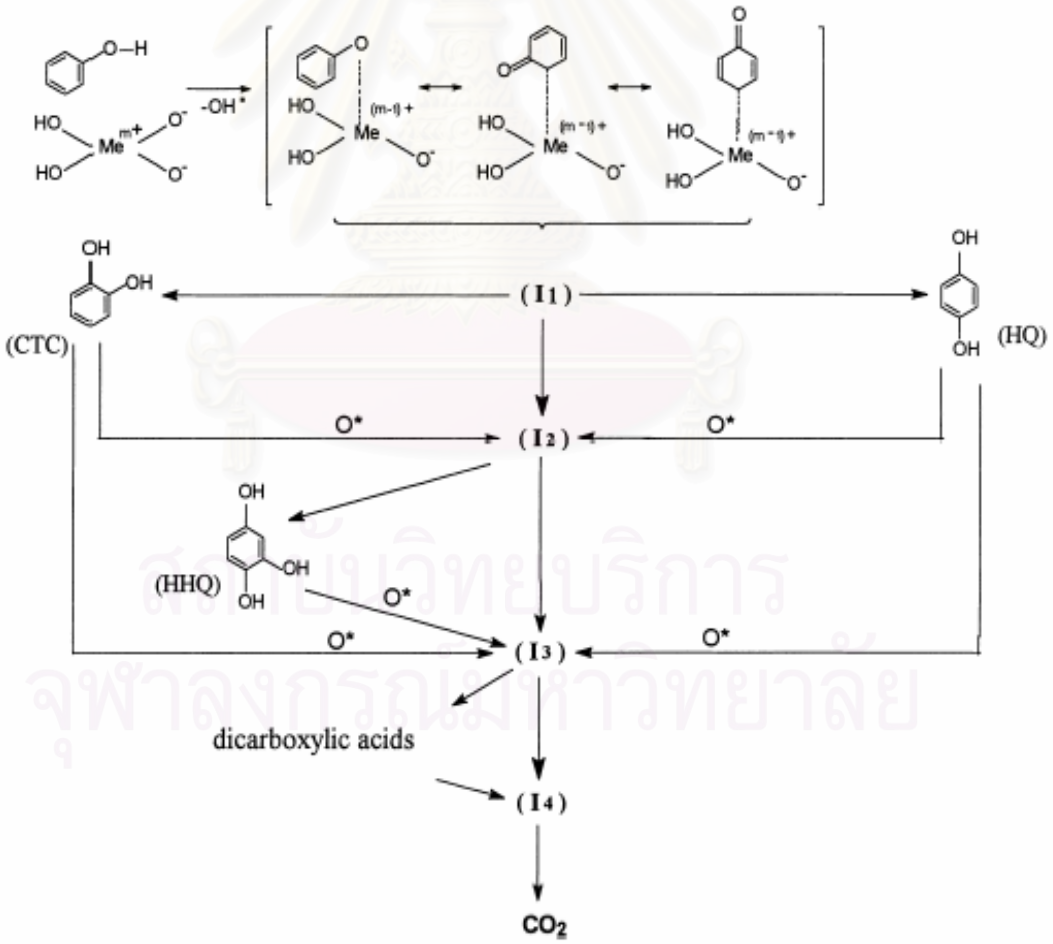

Figure 3.2 Mechanism proposed for the catalytic oxidation of phenol under basic conditions by metallic catalysts [15]

3.2.2 Photo catalytic oxidation [17]

The phenomenon of photocatalysis is probably most often observed in the deterioration of exterior house paints over time as a result of oxidation. Titanium dioxide particles in the paint film use some of the incident solar energy to oxidize organic compounds in that film. Many studies have been carried out on the utilization of this phenomenon for the degradation of toxic pollutants in water, air, and soil.

The major advantages of this technology are as follows:

(i) Photo catalysis offers a good substitute for the energy-intensive conventional treatment methods with the capacity for using renewable and pollution-free solar energy.

(ii) Unlike conventional treatment measures, which transfer pollutants from one medium to another, photo catalysis leads to the formation of innocuous products.

(iii) This process can be used to destroy a variety of hazardous compounds in different wastewater streams.

(iv) It can be applied to aqueous and gaseous-phase treatments, as well as solid- (soil-) phase treatments to some extent.

(v) The reaction conditions for photo catalysis are mild, the reaction time is modest, and a lesser chemical input is required.

(vi) Secondary waste generation is minimal.

(vii) The option for recovery can also be explored for metals, which are converted to their less-toxic/nontoxic metallic states.

The major applications investigated for this technology are removal and destruction of dyes, reduction of COD (chemical oxygen demand), mineralization of hazardous organics, destruction of hazardous inorganics such as cyanides, treatment of heavy metals.

3.2.2.1 Mechanism of photo catalysis [17]

Unlike metals, which have a continuum of electronic states, semiconductors exhibit a void energy region in which no energy levels are available to promote the recombination of an electron and hole produced by photo activation in the solid. The void region that extends from the top of the filled valence band to the bottom of the vacant conduction band is called the band gap (see **Figure 3.3**).

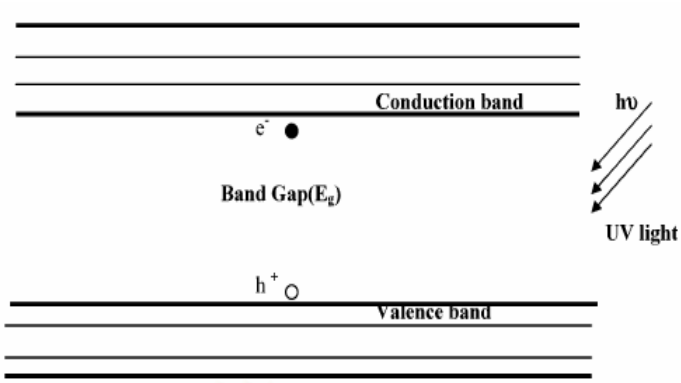

Figure 3.3 Band-gap diagram (formation of holes (h^+) and electrons (e^-) upon UV irradiation of semiconductor surface).

Many materials such as TiO_2, ZnO, ZrO_2, CdS, MoS_2, Fe_2O_3, WO_3, and their various combinations have been examined as photo catalysts for the degradation of organic and inorganic pollutants. The band gaps and physical properties of some semiconductors used in photo catalysis are reported in **Table 3.1**.

Table 3.1 Band-gap energies of semiconductors used for photo catalytic processes [17]

Photocatalyst	band-gap energy (eV)	Photocatalyst	band-gap energy (eV)
Si	1.1	TiO_2 rutile	3.02
WSe_2	1.2	Fe_2O_3	3.1
α-Fe_2O_3	2.2	TiO_2 anatase	3.23
CdS	2.4	ZnO	3.2
V_2O_5	2.7	$SrTiO_3$	3.4
WO_3	2.8	SnO_2	3.5

Absorption of photons by semiconducting solids excites an electron (e^-) from the valence band to the conduction band if the photon energy, $h\nu$, equals or exceeds the band gap of the semiconductor/photocatalyst. Simultaneously, an electron vacancy or a positive charge called a hole (h^+) is also generated in the valence band. Ultraviolet (UV) or near-ultraviolet photons are typically required for this kind of reaction. The electron-hole pair (e^--h^+ pair) thus created migrates to the photocatalyst surface where it either recombines, producing thermal energy, or participates in redox reactions with the compounds adsorbed on the photocatalyst. The lifetime of an e^--h^+ pair is a few nanoseconds, but it is still long enough for promoting redox reactions in the solution or gas phase in contact with the semiconductor. (**Figure 3.4**)

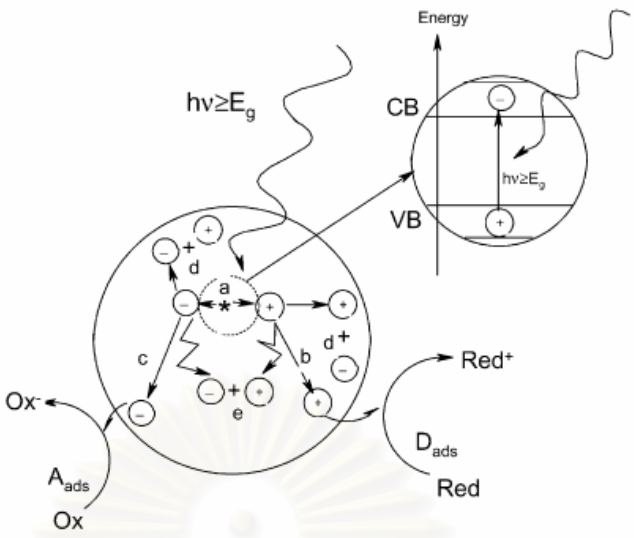

Figure 3.4 Main processes occurring on a semiconductor particle: (a) electron–hole generation; (b) oxidation of donor (D); (c) reduction of acceptor (A); (d) and (e) electron–hole recombination at surface and in bulk, respectively [18]

Generally, the hole oxidizes water to hydroxyl radicals $OH^{\cdot}$ (which subsequently initiate a chain of reactions leading to the oxidation of organics), or it can be combined with the electron from a donor species, depending on the mechanism of the photoreaction. Similarly, the electron can be donated to an electron acceptor such as an oxygen molecule (leading to formation of superoxide radical) or a metal ion (with a redox potential more positive than the band gap of the photocatalyst). This metal ion can be reduced to its lower valence states and deposited on the surface of the catalyst. The electron-transfer process is more efficient if the species are pre-adsorbed on the surface.

3.2.2.2 Photo catalysis based on TiO_2 [19]

Ideally, a semiconductor photocatalyst should be chemically and biologically inert, photocatalytically stable, easy to produce and use, efficiently activated by sunlight, able to efficiently catalyze reactions, cheap, and exhibiting lower risks for the environment or humans. TiO_2 (with sizes ranging from clusters to colloids to powders and large single crystals) is close to being an ideal photocatalyst, displaying almost above properties. The single exception is that it does not absorb visible light.

Both crystal structures, anatase and rutile, are commonly used as photocatalyst, with anatase showing a greater photocatalytic activity for most reactions. It has been suggested that this increased photoreactivity is due to anatase's slightly higher Fermi level, lower capacity to adsorb oxygen and higher degree of hydroxylation (i.e., number of hydroxy groups on the surface).

Photo catalysis based on TiO_2 (anatase) has the following advantages:

– a non-selective destruction of organic and inorganic waste materials may be achieved under normal temperature and pressure in a few hours without production of polycyclic products.

– oxidation of pollutant in ppb range.

– the use of oxygen as the only oxidant.

– capability for simultaneous oxidative and reductive reactions.

– in particular, photo catalysis is known to be effective for inactive substrates such as linear alkanes or their simple derivates, which opens perspectives in oil spill cleaning, elimination of surfactants, and dyes from industrial water.

– these highly active catalysts are adaptable to specially designed reactor systems.

The mechanism of photo catalysis base on TiO_2 for degrading the organic species is presented in the **Figure 3.5**.

$$TiO_2 + h\nu \longrightarrow TiO_2\,(h^+ + e^-) \quad (1)$$

$$O_2 + e^- \longrightarrow O_2^{\cdot -} \quad (2)$$

$$H^+ + H_2O \longrightarrow H^+ + OH^{\cdot} \quad (3)$$

$$OH^{\cdot} + RH \longrightarrow H_2O + R^{\cdot} \quad (4)$$

$$R^{\cdot} + O_2 \longrightarrow ROO^{\cdot} \longrightarrow \longrightarrow CO_2 \quad (5)$$

Figure 3.5 Mechanism of the TiO_2-catalysed UV oxidative degradation of organic species [20]

There are a few researches which specifically studied about the degradation mechanism of phenol by TiO_2. However, Andrzej Sobczyński et.al proposed the research that expresses the mechanism of phenol destruction on illuminated TiO_2 showing in **Figure 3.6** [21].

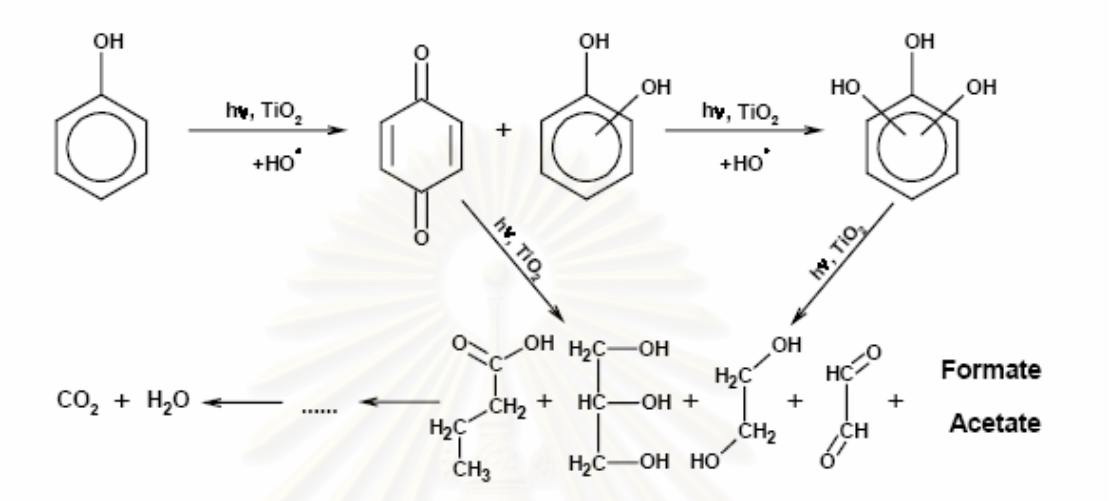

Figure 3.6 A possible mechanism of phenol destruction on illuminated TiO_2.

3.2.3 Ozonation of phenol [22]

Ozone is a very powerful oxidizing agent that can react with most species containing multiple bonds (such as C=C,C=N, N≡N, etc.) It is intensively used in water and wastewater treatment, disinfection, bleaching and industrial oxidation processes. The practical applications are based on the very high oxidizing power of ozone. Ozonation of water and wastewater is carried out by dispersing ozone gas into the liquid phase. Ozone has been employed as oxidants in many water and wastewater treatment applications. Theoretically, ozone should be able to oxidize inorganics to their higher oxidation states while oxidizing organic compounds into carbon dioxide and water. There are two possible ways of oxidizing action in an ozonation process, direct way and radical way.

In the direct way, ozone react directly with phenol molecules and cleavage the ring to finally yield an organic acid molecule as represented in **Figure 3.7** [23].

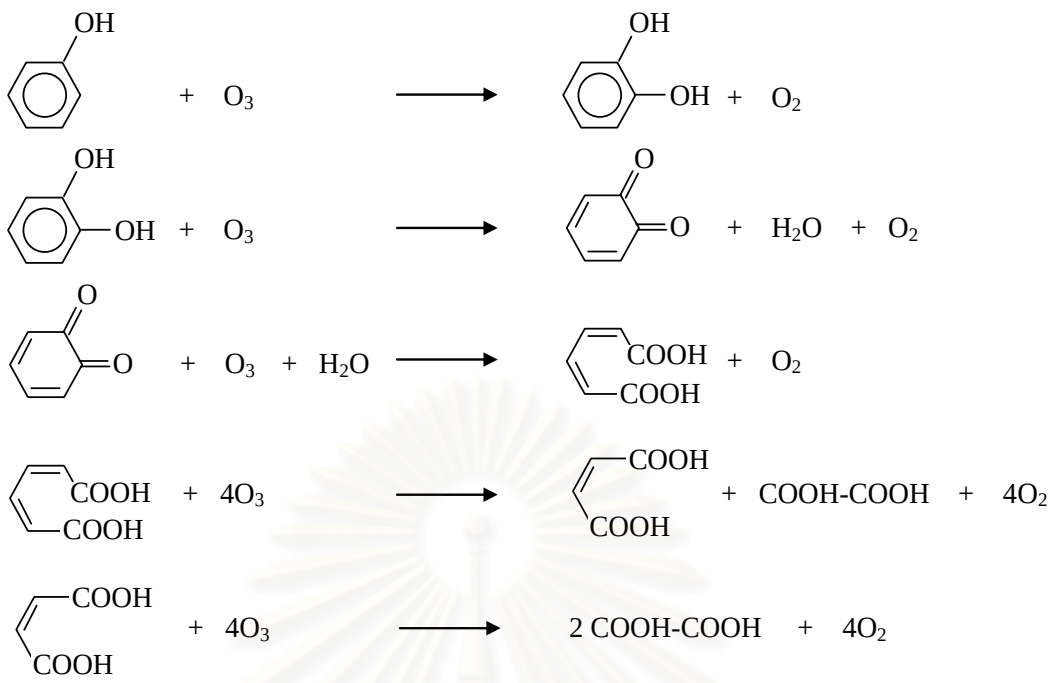

Figure 3.7 Pathways of phenol decomposition by ozonation reaction [23]

Meanwhile the radical way owing to the reactions between the generated radicals, hydroxyl radicals ($OH^{\bullet}$), produced in the ozone decomposition and the dissolved compounds. The global reaction of ozone decomposition to yield hydroxyl radical is [24, 25]:

$$O_3 + H_2O \xrightarrow{h\nu} 2OH^{\bullet} + O_2$$

3.3 Intermediate products of phenol

When phenol is degraded, catechol, hydroquinone and hydroxyl hydroquinone are generated as the products of the initial stage of degradation. These aromatic intermediates undergo to *o*, *p*-benzoquinone and further ring cleavage to yield carboxylic acids such as muconic acid, maleic acid, oxalic acid, etc. which subsequently become CO_2 and H_2O due to decarboxylation. Pathways of the intermediate products were summarized in **Figure 3.8** [6, 26, 27].

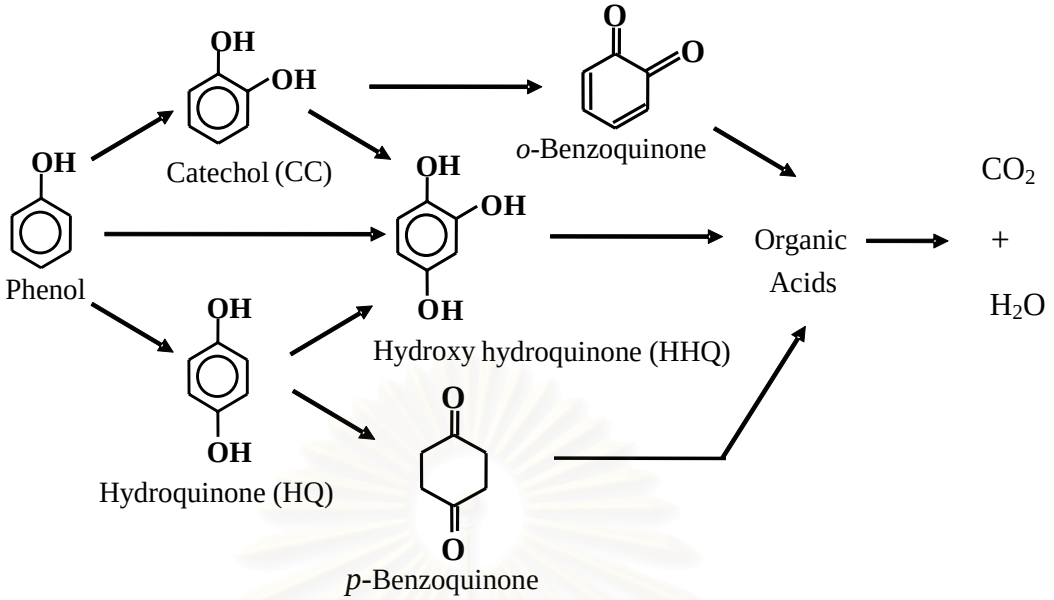
OH
OH
Catechol (CC)
O
O
o-Benzoquinone
OH
Phenol
OH
OH
OH
Hydroxy hydroquinone (HHQ)
Organic
Acids
CO2
+
H2O
OH
OH
Hydroquinone (HQ)
O
O
p-Benzoquinone

(a)

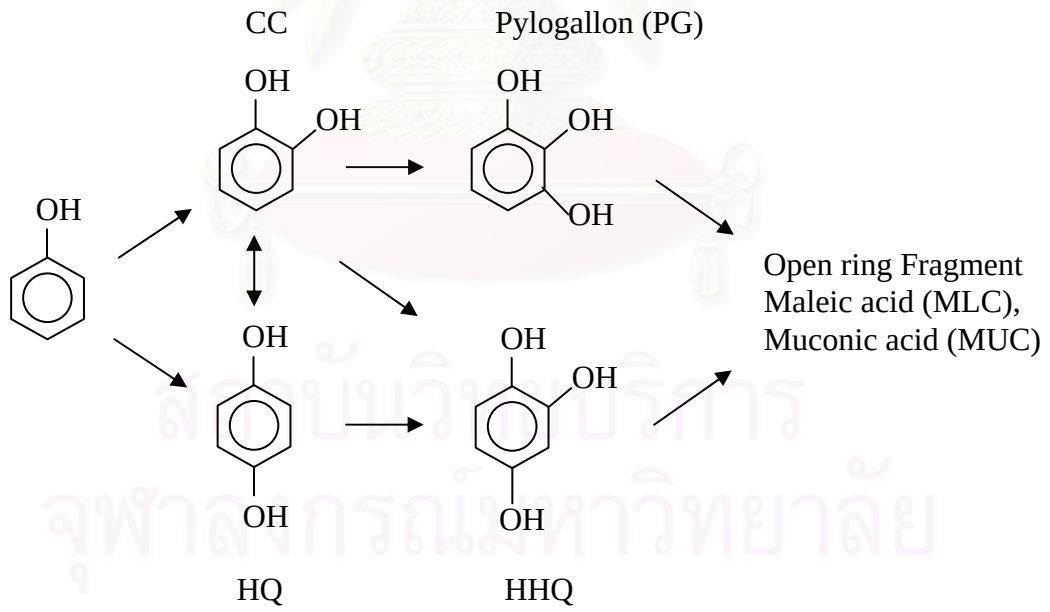
CC
Pylogallon (PG)
OH
OH
OH
OH
OH
OH
OH
OH
OH
OH
OH
Open ring Fragment
Maleic acid (MLC),
Muconic acid (MUC)
HQ
HHQ

(b)

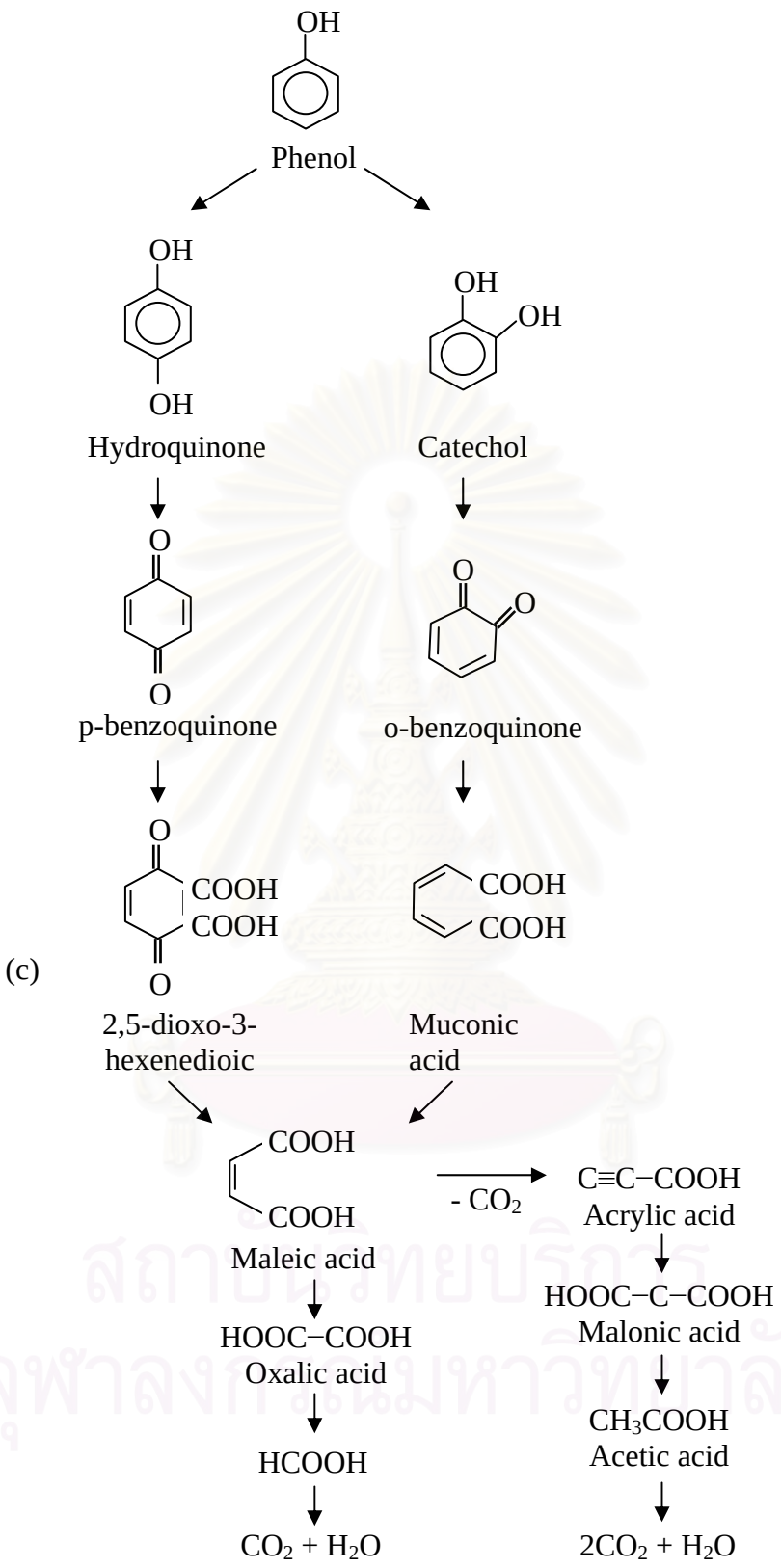

Figure 3.8 Pathways of the phenol intermediate products (a) [9], (b) [26] and (c) [27]

CHAPTER IV

FUNDAMENTAL OF GAS-LIQUID-SOLID FLUIDIZATION

The expression of three-phase fluidization was used to describe fluidization of solid particles by two fluids. A gas and a liquid were the fluidizing media used in the applications. Studies of three-phase fluidization had been of interest and their numerous applications existed in various industrial processes, which varied in size from bench to commercial scale. In such system, the individual phases could be reactants, products, catalysts, or inert. Some examples of three-phase fluidization applications were shown in **Table 4.1**.

Table 4.1 Examples of applications of three-phase fluidized bed processing.

Physical processing	Chemical processing	Biochemical processing
Drying of calcium carbonate and polyvinylchloride	Production of zinc hydrosulfite	Aerobic biological waste treatment
Dust collection	Methanol fermentation	Production of animal cells
Crystallization	Electrode	Enzyme immobilization
Sand filter cleaning	Coal liquefaction	Ethanol fermentation
Drying of granular material	Coal gasification	Antibiotic production
Lactose granulation	Fuel gas desulfurization	Conversing of sucrose to glucose by plant cells

4.1 Gas-Liquid-Solid Fluidization [29]

As mentioned previously, the gas-liquid-solid fluidization was an operation, in which the solid particles layer, fluidized by gas and liquid and then behaved like a fluid. In general, the state of the particle motion in the fluidized bed operation by the upward flow of the fluid could be subdivided into three basic operating regimes: the fixed bed regime, the expanded bed regime, and the transport regime.

The fixed bed regime existed when the drag force on the particle induced by the flow of a gas-liquid mixture was smaller than the effective weight of the particle layer. With an increase in gas and/or liquid velocity, the drag force counterbalances

the effective weight of the particles then the bed would achieve the state of minimum fluidization and marked the onset of the expanded bed regime. With a further increase in gas and/or liquid velocity beyond the minimum fluidization velocity, the solid bed would change to the expanded bed regime until the gas or liquid velocity reached the terminal velocity of the particles in the medium (U_t'). At the gas or liquid velocity above U_t', operation would be considered as the transport regime.

4.2 Hydrodynamics [29]

Hydrodynamic behavior of three-phase fluidized bed reflected, the complex interactions between the individual phases. The most prominent interaction occurred between the rising gas bubbles and the surrounding liquid-solid mixture. Three distinct regions above the gas-liquid distributor were identifiable based on the prevailing physical phenomena: the distributor region, the bulk fluidized bed region, and the free board region. A schematic diagram was shown in **Figure 4.1**.

The distributor region referred to the region immediately above the gas-liquid distributor where gas spouts might occur. It included the region from initial bubble formation to the establishment of the final bubble shape. The hydrodynamic behavior in the distributor region inherently depended on the gas-liquid distributor design and the physical properties of the liquid-solid medium.

The bulk fluidized bed region included the main portion of the fluidized bed. The hydrodynamic behavior in the bulk fluidized bed region varied drastically over large ranges of operating conditions. However, for a given operating condition, there was a minimum axial transport property variation in the region.

Drastically different from the previous regions, the freeboard region mainly contained entrained particles from the bulk fluidized bed region. Particle entrainment led to a solids hold up profile above the fluidized bed surface that decreased axially in a manner similar to that in a gas-solid fluidized bed. Generally, the demarcation between the freeboard region and the bulk fluidized bed region was much more distinct for large/heavy particles than for small/light particles.

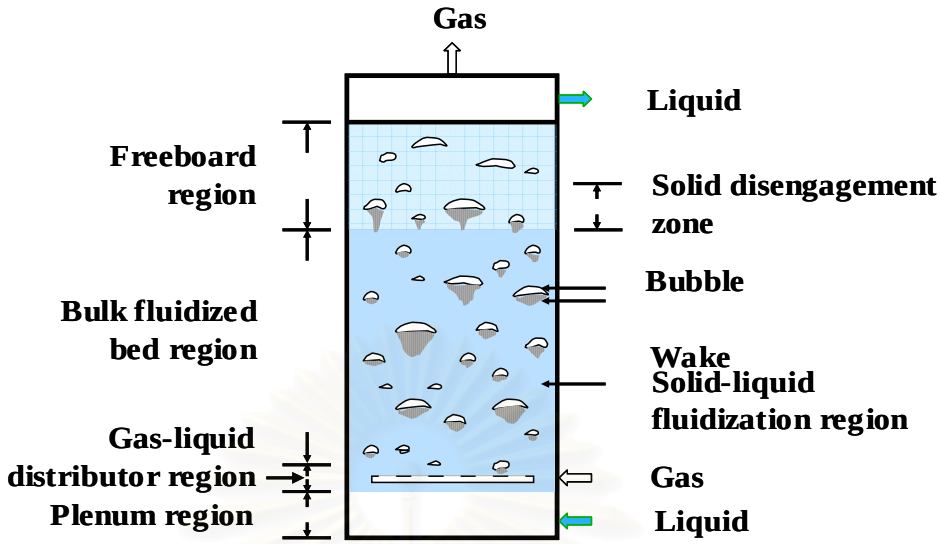

Figure 4.1 Schematic representation of gas-liquid-solid fluidized bed for co-current upward gas-liquid-solid systems with liquid as the continuous phase

4.2.1 Hydrodynamic relations for gas-liquid-solid fluidized bed reactor

A few representative general models of gas-liquid-solid fluidized-bed reactors for the gas phase reactant *A* for a single solid catalyzed reaction $A \longrightarrow$ products are represented in this section. Starting with information about the particle size, density of each phase and viscosity of liquid, the provided hydrodynamic relations may be used to determine bed characteristics such as the minimum fluidization velocity, particle terminal settling velocity, and so on. The equations in this section (4-1 to 4-6) are referred from [30].

Minimum fluidization velocity, U_{mf}

Minimum fluidization velocity was the velocity of fluid, which the solid particles moved apart and few vibrate. The equation for minimum fluidization velocity for gas-liquid-solid fluidized bed reactor was

$$U_{mf} = U_{mf,LS}[1 - 376U_G^{0.327}\mu_L^{0.227}d_p^{0.213}(\rho_S - \rho_L)^{-0.423}] \tag{4-1}$$

$$U_{mf,LS} = \frac{\mu_L(\sqrt{1135.69 + 0.0408Ar} - 33.7)}{d_p\rho_L} \tag{4-2}$$

$$Ar = \frac{\rho_L(\rho_S - \rho_L)gd_p^3}{\mu_L^2} \tag{4-3}$$

where U_{mf} = minimum fluidization velocity (m/s)

$U_{mf,\,LS}$ = minimum fluidization liquid velocity (m/s)

Ar = Archimedes number (-)

U_G = gas velocity (m/s)

μ_L = liquid viscosity (m/s)

d_p = diameter of particle (m)

ρ_S = density of solid (kg/m^3)

ρ_L = density of liquid (kg/m^3)

Terminal velocity, U_t

Terminal velocity of a single particle could be considered with an assumption that the particle moving through a fluid under the action of an external force. If the external force was the acceleration of gravity, *g*, which was constant. Also, the drag force always became larger with an increasing in velocity. The particle quickly reached a constant velocity, which was the maximum attainable under the circumstances, and which was called the terminal velocity. The equation for the terminal velocity was

$$U_t = \frac{gd_p^2(\rho_S - \rho_L)}{18\mu_L} \qquad K < 2.6 \tag{4-4}$$

$$U_t = 1.75\sqrt{\frac{gd_p(\rho_S - \rho_L)}{\rho_G}} \qquad K > 60 \tag{4-5}$$

$$K = d_p\left(\frac{g\rho_L(\rho_S - \rho_L)}{\mu_L^2}\right)^{1/3} \tag{4-6}$$

4.2.2. Pressure Drop and Phase Holdup [31]

When consider a fluidized bed column, which was partly filled with a fine granular material as shown schematically in **Figure 4.2**. The column was opened at the top and had a porous plate at the bottom to support the bed and to distribute the

flow uniformly over the entire cross section. Fluid was admitted below the distributor plate at a low flow rate and passes upward through the bed without causing any particle motion. If the particles were quite small, flow in the channels between the particles would be laminar and the pressure drop across the bed would be proportional to the superficial velocity. As the fluid velocity was gradually increased, the pressure drop increased, but the particles did not move and the bed height remained the same. At a certain velocity, the pressure drop across the bed counterbalances the force of gravity on the particles or the weight of the bed, and any further increase in velocity caused the particles to move. This was point A on the graph. Sometimes the bed expanded slightly with the grains still in contact, since just a slight increased in porosity, ε could offset an increase of several percent in superficial constant and keep pressure drop, ΔP constant. With a further increase in velocity, the particles became separated enough to move above in the bed, and true fluidization begins (point B).

Once the bed was fluidized, the pressure drop across the bed became constant, but the bed height continues to increase with increasing flow. The bed could be operated at quite high velocities with very little or no loss of solids, since the superficial velocity needed to support a bed of particle was much less than the terminal velocity for individual particles.

If the flow rate to the fluidized bed was gradually reduced, the pressure drop remained constant, and the bed height decreased, following the line BC that was observed for increasing velocities. However, the final bed height might be greater than the initial value for the fixed bed, since solids dumped in a column tended to pack more tightly than solids slowly settling from a fluidized bed state. The pressure drop at low velocities was then less than in the original fixed bed. On starting up again, the pressure drop offset the weight of the bed at point B, and this point, rather than point A, should be considered to give the minimum fluidization velocity, U_{mf} To measure U_{mf}, the bed should be fluidized vigorously, allowed to settle with the fluid turn off, and the flow rate increased gradually until the bed starts to expand. More reproducible value of U_{mf} could sometimes be obtained from the intersection of the graphs of pressure drop in the fixed bed and the fluidized bed.

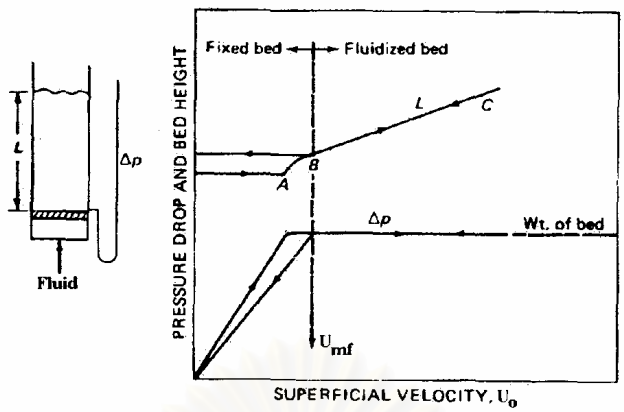

Figure 4.2 Pressure drop and bed height and superficial velocity for a bed of solid. (Redrawn from *McCabe et al*, Unit operation of chemical engineering. 1993, p.1 65)

The pressure drop through the bed was strongly related to the individual phase holdup in the bed. The phase holdup was defined as the fraction of the solids, liquid or gas phase to volume of the column. In the fluidized bed section with low solids entrainment rates, the solid holdup, ε_s, could be expressed as

$$\varepsilon_s = \frac{W}{\rho_s SH} \tag{4-7}$$

However, behavior of gas holdup in the freeboard region strongly depended on the flow regimes and hence, on both particle and liquid properties. Gas holdup in three-phase fluidized beds could be lower than that in a corresponding bubble column because the particles promoted bubble coalescence, however it could also be higher than that in a corresponding bubble column when the particles helped break up gas bubble in some certain operating ranges. Furthermore, gas holdup was important for determining residence time of the gas in liquid. Kato et al. (1985) had proposed that the gas holdup in a system of gas-liquid-solid fluidization could be approximated by the following equation;

$$\varepsilon_g = \frac{0.3W^{1.3}}{(1+1.1W^{1.15})} \tag{4-8}$$

when the parameter W was defined as

$$W = \left(\frac{gD_c^2\rho_L}{\sigma}\right)^{0.196}\left(\frac{gD_c^2}{\mu_L^2}\right)^{0.035}\left(\frac{U_G}{\sqrt{gD_c}}\right) \tag{4-9}$$

The following relationship held among individual holdups:

$$\varepsilon_G + \varepsilon_L + \varepsilon_S = 1 \tag{4-10}$$

Under the steady state condition, the total axial pressure gradient (static pressure gradient) at any cross section in the column represented the total weight of the bed consisting of the three phases per volume as given by

$$g\frac{-dP}{dZ} = (\varepsilon_G\rho_G + \varepsilon_L\rho_L + \varepsilon_S\rho_S)d \tag{4-11}$$

where $\varepsilon_G, \varepsilon_L, \varepsilon_S$ = gas, liquid, and solid holdup (-), respectively.

$\rho_G \rho_L \rho_G$ = gas, liquid, and solid density (kg/m^3), respectively.

W = weight of solid particle in the bed (kg).

S = cross-section area of empty column (m).

H = effective height of bed expansion (m).

g = gravitational acceleration (m/s^2).

$\frac{dP}{dZ}$ = static pressure gradient.

D_c = column diameter (m)

σ = surface tension (mN/m)

μ_L = kinematic liquid viscosity (m^2/s)

U_G = gas velocity (m/s)

The frictional drag on the wall of the column and the acceleration of the gas and liquid flows could be neglected. In equation (4-11), the term $\varepsilon_G\rho_G$ in the right hand side was usually negligibly small compared to the other terms. The evaluation of

individual phase holdups based on the pressure gradient method, ε_S could be directly obtained from equation (4-7) with the height of bed expansion measured experimentally while ε_G could be directly calculated from equation (4-8). Finally, ε_L could be calculated from equation (4-10) and (4-11) simultaneously with the experimentally measured static pressure gradient.

4.2.3. Flow Regime

Three flow regimes could be identified based on the bubble flow behavior in three-phase fluidized bed: the coalesced bubble, the dispersed bubble, and the slugging regimes. In the coalesced bubble regime, bubbles tended to coalesce and both the bubble size and velocity became large and shown a wide distribution. Coalesced bubbles rose near the column near the column center with high velocity and stirred the bed violently. The coalesced bubble regime predominated at low liquid and high gas velocities. In the dispersed bubble regime, no bubble coalescence occurred and the bubbles were of uniform, small size. The dispersed bubble regime predominated at high liquid velocities and at low and intermediate gas velocities. In a small diameter column (e.g., D_c < 15 cm), the gas bubble could easily grew to the size of the column diameter at high gas flow rates creating “slug” bubbles which occupied nearly the whole cross section. In columns of large diameter, however, slugging might not occur. The flow regimes varied significantly with the column diameter. Particle properties also profoundly affected the prevailing flow regime at given gas and liquid velocities and terminal velocity of the fluidized particles affected the liquid velocity of transition from the coalesced to the dispersed bubble regime

CHAPTER V

EXPERIMENTAL

This chapter describes the experiment in details. The chemicals, the catalysts and the experimental system are shown in sections 5.1, 5.2 and 5.3, respectively. In sections 5.4, 5.5, and 5.6, the equipment, the experimental procedure and analytical instrument are explained.

5.1 Chemicals

Phenol and intermediate products solution, hydroquinone and catechol, for testing the reaction and preparing HPLC standard are prepared from:

1) Phenol, C_6H_6O, available from Polski Odczynniki Chemiczne S.A., 99.9%
2) Pyrocatechol, $C_6H_6O_2$, available from Fluka, 98%
3) Quinol, $C_6H_4(OH)_2$, available from APS Chemicals, 99.8%

In addition the HPLC mobile phase, Acetonitrile, is:

4) Acetonitrile, CH_3CN, available from Fisher Scientific, 99.99%

5.2 Catalysts

There are two types of catalyst for testing in this research. First is photocatalyst and second is metallic catalyst. The photocatalyst, a commercial TiO_2 on silica bead, was obtained from Fuji Silysia Chemical Ltd. The metallic catalysts, nickel (Ni) or cobalt (Co) on mesoporous carbon bead, were prepared by Dr. Takuji Yamamoto from national institute of Advanced Industrial Science and Technology (AIST), Japan with sol-gel method.

5.3 Experimental system

5.3.1 Lab scale system

First, lab scale system was set up. The main equipment consist of hold up tank, magnetic stirrer, liquid pump, flow meter, 3-way valve, ozone generator, oxygen tank, UV-lamp and lab scale 3-phase fluidized bed reactor. All the equipment was composed as show in diagram in **Figure 5.1.**

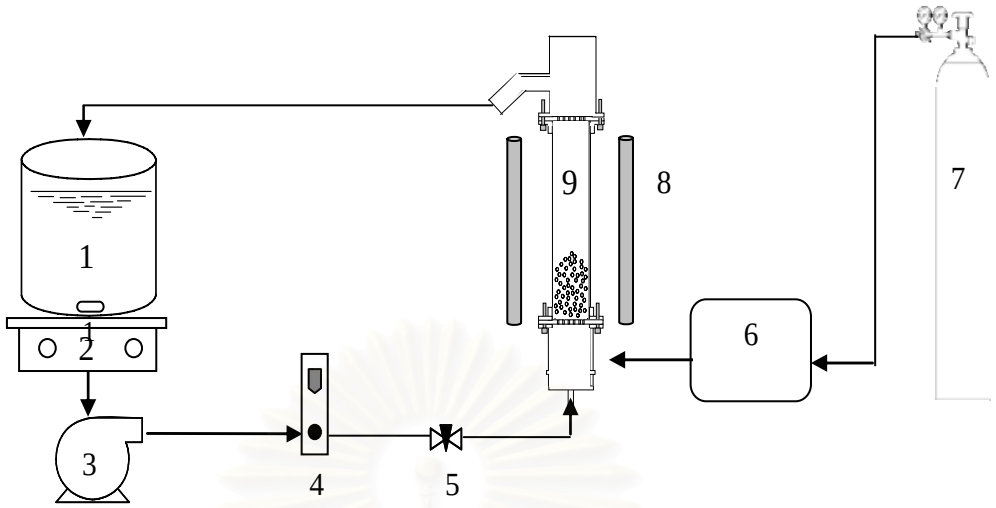

Figure 5.1 Diagram of equipment set up for circulated system**;** 1.hold-up tank (T1), 2.magnetic stirrer, 3.liquid pump, 4.flow meter, 5.3-way valve, 6.ozone generator, 7.oxygen tank, 8.UV-lamp and 9.lab-scale 3-phase fluidized bed reactor

5.3.2 Pilot scale system

In pilot-scale, the reactors were constructed and set up in series. (see the schematic diagram of equipment in **Figure 5.2**). This system consists of five reactor columns (V1-V5), two wastewater preparation tanks (T0, T1), four water tanks (T2-T5), a treating tank (T6) and six chemical resistant pumps with the same specifications. For the water stream, there are liquid flow meters to measure the inlet wastewater flow rate of each column. Two wastewater preparation tanks are set because one of them will be used to prepare the wastewater while the other is used during the operation. The evaporated water in the system should be negligible so the make-up water is not necessary in this system. For the gas stream, commercial grade oxygen is employed to produce ozone. Total gas flow rate is equally separated into 5 lines for distribution to each column. Before entering each column, the gas flow meters are used to adjust flow rate. The ozone-oxygen mixture is passed through the ceramic distributor to reduce size of gas bubbles in the column, leading to an increased contact area of the reactants. The check valves are also set below each column for preventing the damage of gas flow meters due to the water inside column back flowing into the ozone flow meters.

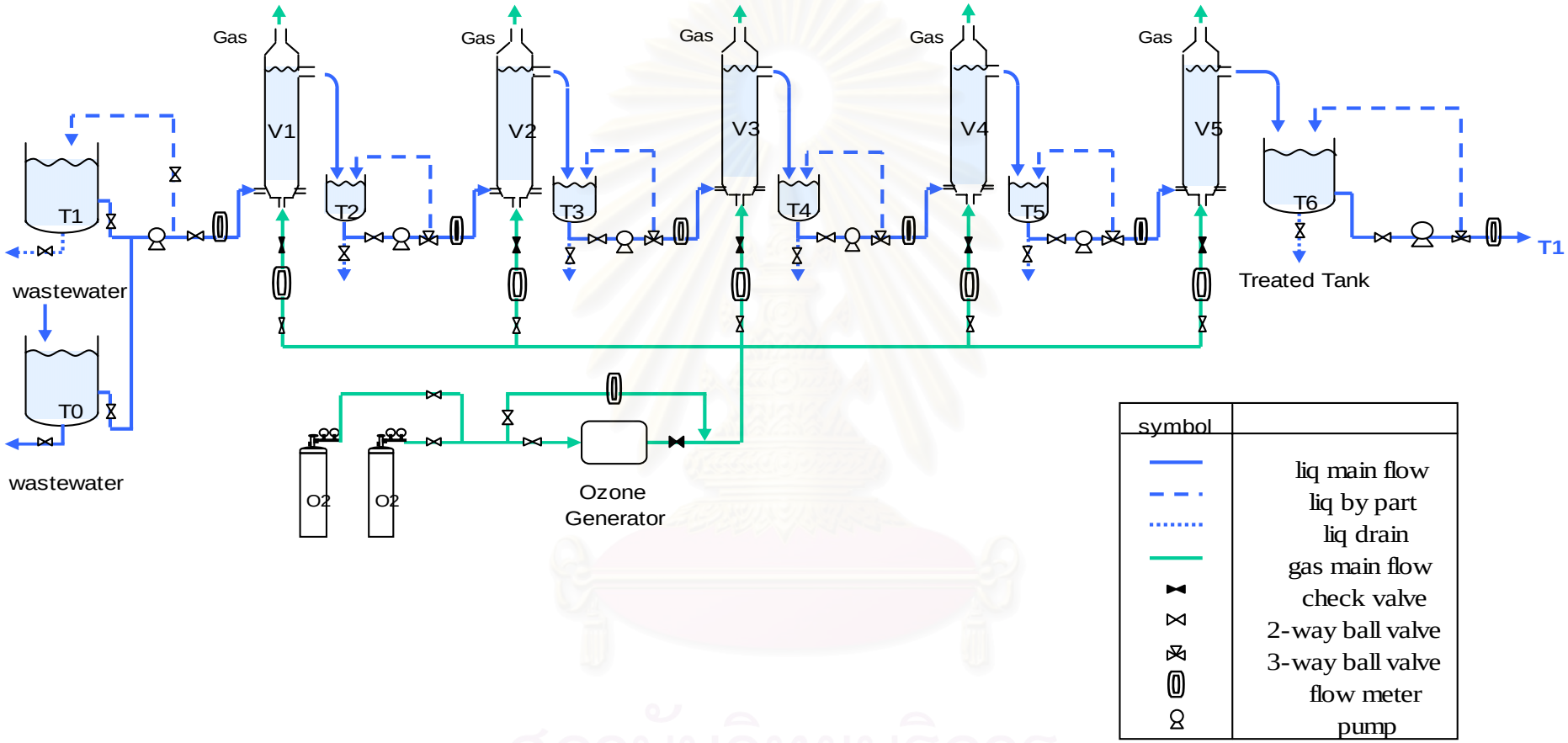

Figure 5.2 Schematic flow diagram of the designed pilot-scale process

5.4 Equipment

5.4.1 Lab scale equipment

Reactor

The reactor is made from acrylic while the central portion of the reactor is made of quartz tube to allow the irradiation from UV-lamps to reach the fluidized photocatalyst beads. It has effective volume 235 mL, 31.6 mm in inside diameter and 300 mm in high.

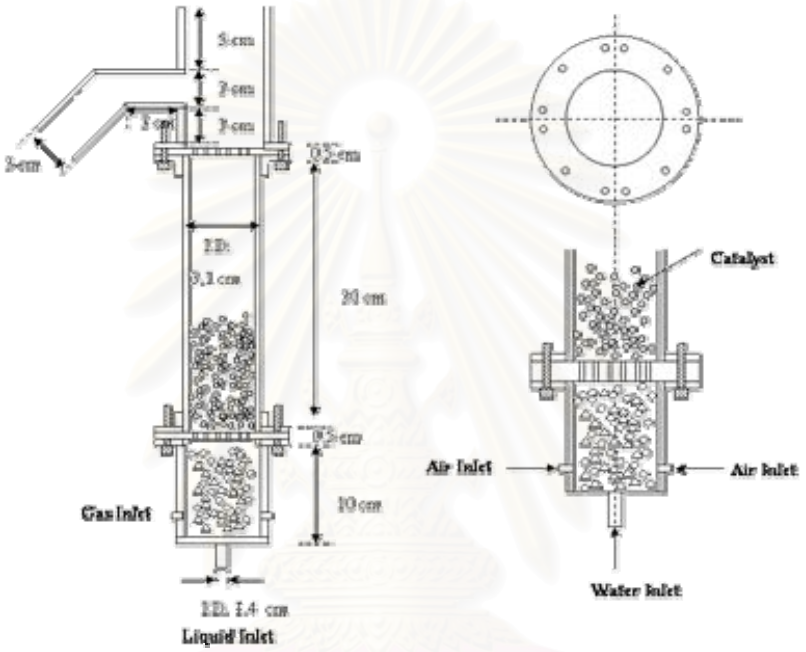

Figure 5.3 Construction diagram of a lab-scale fluidized bed reactor

Figure 5.4 Photo of lab scale fluidized bed reactor

UV-lamps

Two UV-C lamps (Philips TUV 15W, λ = 254 nm) are light source for this system when operating by photocatalyst.

Ozone generator

Figure 5.5 is shows a photo of the ozone generator model SO-O3UN-OX. Its technical specifications are shown in **Table 5.1.** This apparatus uses oxygen or air as a source of ozone production. When oxygen is used, a much higher ozone production rate could be obtained. Moreover, the gas flow rate can be varied in the range of 1-5 L/min., and the ozone generation rate is between 1.4-5.7 g/h depending on the gas flow rate. The ozone concentration slightly decreases with an increase in gas flow rate.

Figure 5.5 Ozone generator model SO-O3UN-OX of Tokyu Car Co., Ltd

Table 5.1 Specification of the ozone generator model SO-O3UN-OX

Oxygen flow rate [L/min.]	**O_3 concentration [g/m^3]**	**O_3 generation rate [g/h]**
1	24.39	1.46
2	22.73	2.73
3	21.29	3.83
4	19.85	4.76
5	18.77	5.63

Model: SO-03UN-OX03007, Source: Oxygen (O_2), Oxygen flow rate: 1-5 L/min., Room temperature: approx. 23 ^{o}C, Room humidity: approximately 70%, Pressure of supplied oxygen: 2 kg$_f$/cm^2.

5.4.2 Pilot scale equipment

Reactor

The design parameters of pilot scale three-phase fluidized bed reactor are shown in **Table 5.2**. These reactors were made from transparent acrylic. The shape of the top of reactor was designed like a conical shape to reduce dead volume above the liquid surface as much as possible. At the bottom of the column, three pipes were built for water draining, gas inlet, and water inlet, respectively (see **Figure 5.6**).

Table 5.2 Design parameters of the pilot-scale fluidized bed reactor

Effective volume of each reactor	50 L
Outer diameter of each reactor	0.2 m (I.D. = 0.19 m)
Height of each reactor	Approx. 2 m (effective height 1.6 m)
H/D ratio (height of water/ diameter of reactor)	8
Amount of catalyst	51 g per each reactor

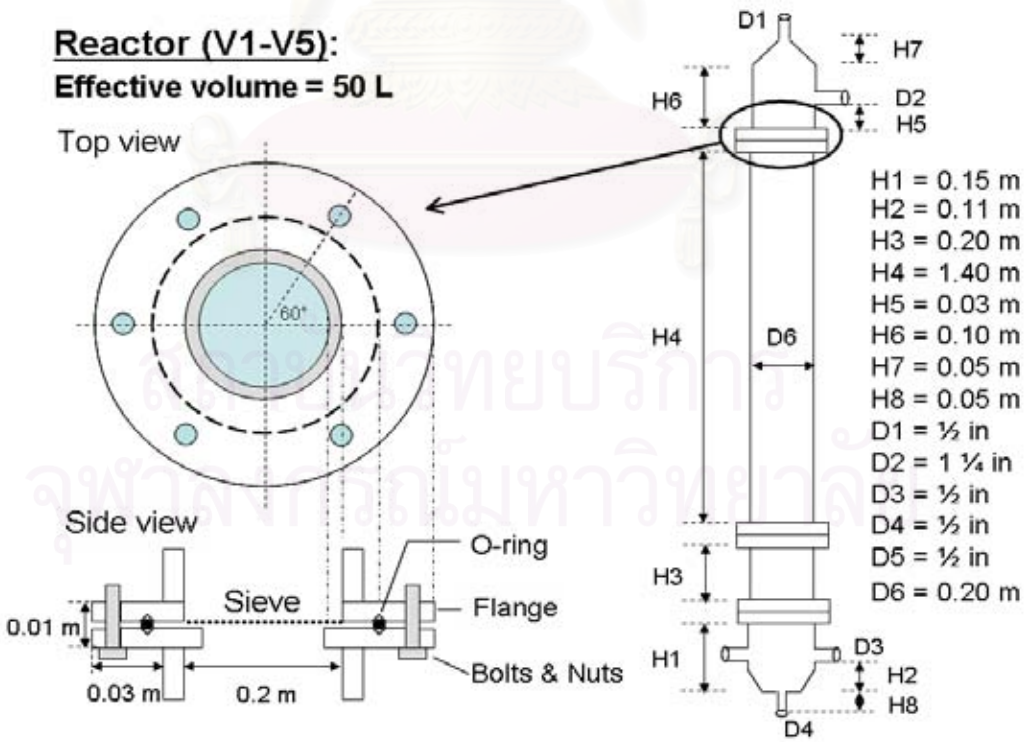

Figure 5.6 Design configurations of three-phase fluidized bed reactor in the pilot-scale system

(a)

(b)

Figure 5.7 Photos of the pilot-scale three-phase fluidized bed reactors

Ozone generator

1) Ozone generator from Walailuck University

The appropriate gas flow rate for Walailuck University ozone generator, shown in **Figure 5.8,** is 15 L/min which gives the ozone generation rate equal to 16 g/h. The unit generates ozone with high frequency corona discharge in 6 separately pathways and cools the plasma system by cooling water.

Figure 5.8 Walailuck University ozone generator

2) Ozone generator model OZ-754 of Asia-Tech Engineering Co., Ltd

Figure 5.9 Ozone generator model OZ-7540 of Asia-Tech Engineering Co., Ltd

Table 5.3 Technical data of ozone generator model OZ-7540

Model	OZ-7540
Ozone capacity (max)	40 g/h
Air flow rate (max)	40 L/min
Operating function	Manual / Auto
Power consumption	2.2 kW.
Ozone concentration	3 % by weight from dry air
Power supply	380 VAC, 50 Hz
Type of generating mechanism	High frequency Corona discharge
Type of cooling system	Water cooled
Type of electrode	Stainless steel 316 L with glass tube
Type of ozone tube	Teflon tube
Type of fitting	Stainless steel 316
Type of cabinet	Steel with epoxy paint
Ozone unit dimension (WxHxD)	600 x 1700 x 500 mm.
Chiller dimension (WxHxD)	530 x 700 x 530 mm.
Weight	310 kg.

5.5 Experimental procedure

For lab-scale

All experiments were carried out with co-current upward flow of gas and liquid. For batch experiment, the phenol-containing liquid and/or ozone-containing gas were fed in at the bottom, flew out from the top and the entire liquid was re-circulated via the hold-up tank. But for continuous running the entire liquid from the top of the reactor was drained out.

For pilot-scale

The experiments in pilot scale system were carried out with co-current upward flow same as in lab-scale system. However, instead of passing through just one reactor, the liquid had flown through five reactors in series. The entire liquid from last reactor was re-circulated via the preparation tank until finish.

5.6 Analytical instrument

It is necessary to analyze the catalyst characteristics. This information renders the better understanding of the phenomena which has an impact on discussion to be tranceworthy. The devices for examining consist of the gas chemisorption (H_2 and CO), nitrogen physisorption and XRD. Moreover, after the treating time phenol will be decomposed to intermediate products and becomes to carbon dioxide and water finally. HPLC and TOC are the tools for the analyzation. The details of the equipment are described next.

5.6.1 Gas chemisorption

H_2 chemisorption was carried out following the procedure described by Reuel and Bartholomew using a Micromeritics Pulse Chemisorb 2750 system. Prior to H_2 chemisorption, approximately 0.2 gram of the catalysts were reduced at 350°C after ramping at a rate of 10 ^{o}C min^{-1} and held at that temperature for 3 h. Static H_2 chemisorption was performed at 100 ^{o}C.

CO chemisorption was carried out following the procedure described by Reuel and Bartholomew using a Micromeritics Pulse Chemisorb 2750 system. Prior to CO chemisorption, approximately 0.2 gram of the catalysts were reduced at 400°C in H2 atmosphere after ramping at a rate of 10 ^{o}C min^{-1} and held at that temperature for 0.5 h. Static CO chemisorption was performed at 30 ^{o}C.

5.6.2 Nitrogen physisorption

The sample's Brunauer-Emmett-Teller (BET) surface area was determined by nitrogen adsorption in a BEL Japan Inc., model (BelSorp 2).

5.6.3 X-ray diffraction spectroscopy (XRD)

XRD was performed to determine crystal phase, bulk crystallinity, and crystallite size of metal catalyst. It was conducted using a SIEMENS D5000 X-ray diffractometer with Cu K_α radiation (λ = 1.54439 A^o) with Ni filter. The spectra were scanned at a rate of 0.04^o min^{-1} in the 2θ range of 20-80°. The crystallite size was estimated from line broadening according to the Scherrer equation (see Appendix A) and α-Al_2O_3 was used as standard.

5.6.4 High performance liquid chromatography (HPLC)

The concentration is measured by HPLC (Shimadzu column class VP). It can be used for indicating the compounds and the number of the compounds in the sample as well. The result from the sample taken in sequent of time is exhibited in graph form. Peak area of each compounds occurred at the individual resident time were brought to calculate the concentration. In addition the degradation time of each batch can be found by HPLC. 25% acetonitrile : 75% demineralized water (conductivity < 2 microziemen) were mobile phase. The total flow rate of mobile phase was 0.6 cm^3/min. The column Phenomenex C18 was operated at 31.5 °C. The wavelength of UV-vis detector was 254 nm. **Figure 5.10** shows the picture of this tool.

Figure 5.10 The picture of HPLC (Shimadzu column class VP)

5.6.5 Total organic carbon (TOC)

The TOC disappearance was obtained from Shimadzu TOC-VCPH. It could be used for indicating the total mineralization of phenol. The picture of TOC analyzer is shown in **Figure 5.11**.

Figure 5.11 The picture of TOC analyzer (Shimadzu TOC-VCPH)

CHAPTER VI

RESULTS AND DISCUSSIONS

TiO_2 photocatalyst, nickel and cobalt metallic catalysts are employed for investigating the phenol decomposition efficiency and the possibility of the lab-scale fluidized bed reactor for application on wastewater treatment.

6.1 Catalyst characteristics

The photocatalyst, a commercial TiO_2 on silica bead, and its characteristics showing in **Table 6.1** were obtained from Fuji Silysia Chemical Ltd.

Table 6.1 The characteristics of TiO_2 on silica bead

Properties	Value
Diameter (mm)	0.85-1.70
TiO_2 content (%wt)	9.6-12.5
Pore volume (mL/g)	0.84
Specific surface area (m^2/g)	325

Meanwhile the metallic catalysts, nickel (Ni) or cobalt (Co) on mesoporous carbon bead, were prepared by Dr. Takuji Yamamoto from National institute of Advanced Industrial Science and Technology (AIST), Japan with sol-gel method.

Most characteristic of the catalysts in **Table 6.2** (except the crystalline size) were obtained from AIST. The XRD pattern in **Figure 6.1,** crystalline size in **Table 6.2,** and metal active site in **Table 6.4** and **Table 6.5** were supported by Center of Excellence on Catalysis and Catalytic Reaction Engineering, Department of Chemical Engineering, Faculty of Engineering, Chulalongkorn University.

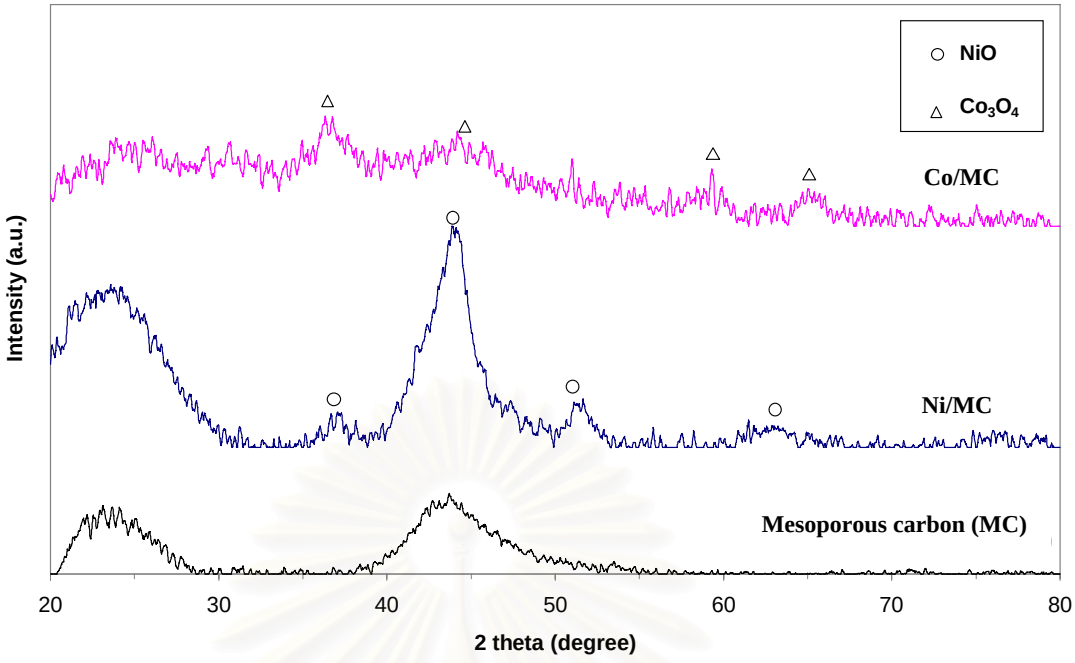

Figure 6.1 The XRD patterns of the Ni and Co metallic catalyst

The crystalline structure of cobalt and nickel metallic catalyst was examined by the X-ray diffraction patterns. As shown in **Figure 6.1**, series of typical peaks at 2θ = 37.0◦, 45.0◦ and 65.4◦, respectively, which are attributed to the characteristics of Co_3O_4 [32], can be easily observed in Co/MC sample. The other cobalt oxides (such as CoO and Co_2O_3 so on) are absent. For Ni/MC, the nickel oxide (NiO) are also observed at 2θ = 36.9◦, 43.5◦ and 62.5◦. [33]

The BET surface areas, diameter of catalyst bead, crystalline size of metal are shown in **Table 6.2**. The BET specific surface area of the samples was calculated to be ca. 736-784 m^2/g. It can be observed that a pure activated carbon support gives a more BET surface area than the activated carbon supported metallic catalyst. This indicates the plugging of the loaded metal on the activated carbon pore. The crystalline size of the cobalt metallic catalyst calculated from the Scherrer's equation was approximately 2.4 nm, while that of the nickel metallic catalyst was 3.0 nm.

Table 6.2 The characteristics of Ni or Co on mesoporous carbon bead

Catalyst	Diameter (mm)	BET surface area (m^2/g)	Carbonized temperature (^oC)	Mesopore volume (mL/g)	Crystalline size (nm) [a]
Mesoporos carbon (MC)	0.6	784	600	1.55	-
5 %wt Co/MC	0.6	736	600	1.23	2.4
5 %wt Ni/MC	0.6	761	600	1.49	3.0

[a] Calculated from Scherer's equation

6.2 Possibility of TiO_2 photocatalyst for phenol degradation by the lab-scale fluidized bed reactor

When TiO_2 photocatalyst is irradiated with ultraviolet light (λ<390 nm), a strong oxidizing agent such as hydroxyl radicals will be produced. These radicals will attack some organic molecules which are adsorbed on or existing close to the surface of the catalyst, thus leading to degradation into small inorganic species. The information and mechanism of the process are already explained in chapter III.

Other photocatalysts, which have been reported, are WO_3, $SrTiO_3$, α-Fe_2O_3 ZnO and ZnS. However, those catalysts are not attractive for environmental application when compared with anatase TiO_2 because TiO_2 is biologically and chemically inert, inexpensive and resistant to photo corrosion and chemical corrosion [34].

6.2.1 Effect of catalyst loading

At the beginning, the experiment was carried out in the system without gas feeding to find out the appropriate amount of catalyst by varying the catalyst loading (2.5, 5, 10 and 20 g, respectively) with constant liquid flow rate of 1 L/min.

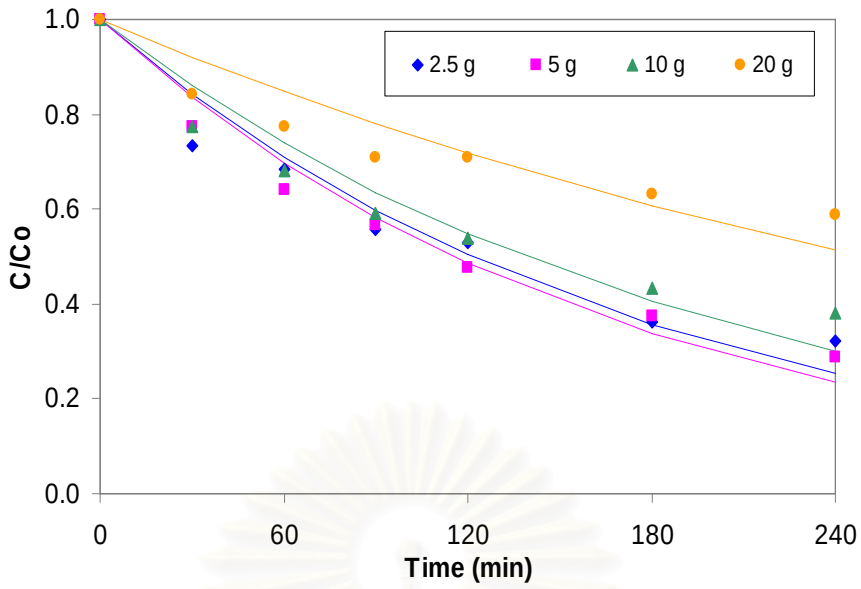

Figure 6.2 Effect of dosage of TiO_2 catalyst (9.6 %wt TiO_2 content) in a 2-phase FBR

Data of the optimal loading of catalyst is desirable for effective operation of photocatalytic systems. The optimal loading depends on the type and dimensions of the reactor being used as well as on the kind of pollutants. **Figure 6.2** shows that the degradation efficiency slightly increased as the catalyst loading was doubled from 2.5 to 5 g. However, an increase in the loading over 5 g instead results in the decreasing removal efficiency. Similarly, it was reported that the rate of phenol oxidation initially increased with the concentration of TiO_2 before reaching a maximum level. Thereafter, the oxidation level decreased to a constant value upon further increase in TiO_2.

Additionally, *Chen et al.* [35] suggested that an increase in fluid opacity and light scattering by TiO_2 particles progressively occurred at a higher catalyst loading, leading to the hindered passage of irradiation through the sample. The optimal amount of TiO_2 on silica beads was found to be around 5 g of catalyst.

6.2.2 Effect of ozone on degradation rate

To study the effect of ozone on the degradation of phenol, 5 g of photocatalyst (12.5 %wt TiO_2 content.) was used to decompose 2 L of 10 ppm aqueous phenol with liquid flow rate of 1 L/min. The ozone was generated from air at the constant flow rate of 1 L/min.

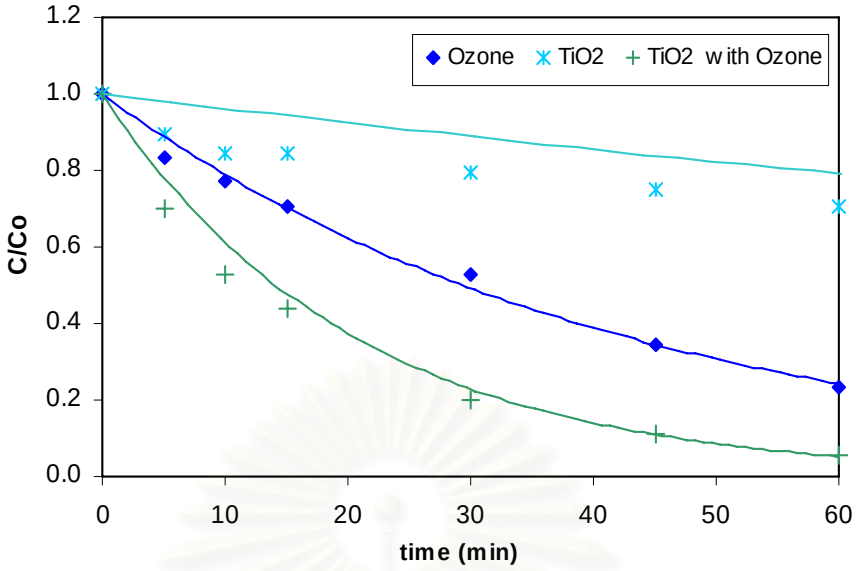

Figure 6.3 Effect of ozone on the degradation of phenol

In **Figure 6.3** it could be observed that when only TiO_2 catalyst was employed it could give rise to the lowest degradation efficiency. In other words, it took a long operating time, approximately 8 h, to decompose the phenol concentration from 10 ppm to less than 1 ppm. In contrast, when TiO_2 catalyst was employed with feeding of ozone (generated from air) the system could provide a higher efficiency. Therefore it could be supposed that addition of ozone will increase phenol degradation efficiency.

Santiago Esplugas et al. [24]. has reported that there are two possible ways of oxidizing action, which are direct way and radical way. In the direct way, ozone reacts directly with phenol molecules and cleavage the ring to finally yield an organic acid molecule as represented in **Figure 3.7**.

The experimental results shown in **Figure 6.3** can be interpreted in terms of conversion with respect to decomposition term (see **Table 6.3**). Phenol conversion, X_{Ph}, is defined as:

$$X_{Ph} = \frac{[Ph]_0 - [Ph]_t}{[Ph]_0} \times 100$$

Table 6.3 The conversion of phenol by TiO_2, ozone, and TiO_2 with ozone.

Method	Conversion of phenol at time					
	5 min	10 min	15 min	30 min	45 min	60 min
TiO_2 (12.5% wt)	10.75	15.28	15.79	20.61	24.97	29.18
Ozone	16.54	22.64	29.35	47.22	65.42	76.44
TiO_2 (12.5% wt) with ozone	29.79	47.01	56.19	79.95	88.87	94.17

The decomposition of phenol by TiO_2, ozone and TiO_2 with ozone are denoted as X_a, X_b and X_c, respectively. In the first 30 minute, the conversion for the last case (TiO_2 with ozone) was higher than the combined conversions of the first two cases of using either only ozone or only TiO_2 ($X_c > X_a+X_b$). Then, at t equal 45 min, the conversions of the last system became slowly decreased ($X_c < X_a+X_b$). It might be concluded that, by adding ozone, the overall degraded reactions are not only photocatalytic reaction and ozonation (direct way) but also consist of the synergistic interactions (radical way) which occur from generated radicals ($OH^{\bullet}$) produced in the ozone decomposition.

According to the theory of ozonation in chapter III, ozone under UV light ($\lambda<330$) helped producing hydroxyl radical ($OH^{\bullet}$). Therefore the conversion X_c in the first period is more than X_a+X_b. However after this initial period, majority of phenol in the solution would already be decomposed. Thereafter, there was not enough phenol for all degraded reactions and the conversion X_c will become less than X_a+X_b.

6.3 Possibility of metallic catalyst for phenol degradation by lab-scale fluidized bed reactor

To investigate the possibility of metallic catalyst applications for wastewater treatment, the metallic catalyst was tested in a lab-scale fluidized bed reactor (FBR) for treating phenol solution. The metallic catalysts used in this project were Ni - metallic catalyst and Co - metallic catalyst.

6.3.1 Comparative catalytic activity between cobalt and nickel catalyst

To compare the initial catalytic activity between Co and Ni catalysts in the 3-phase FBR, the selected operating conditions are the same as the case of phenol degradation by TiO_2 with ozone (5 g of catalyst loading and 1 L/min of liquid and gas flow rate). The catalytic degradation of phenol at two different phenol concentrations (10 ppm and 100 ppm) is presented in **Figure 6.3**.

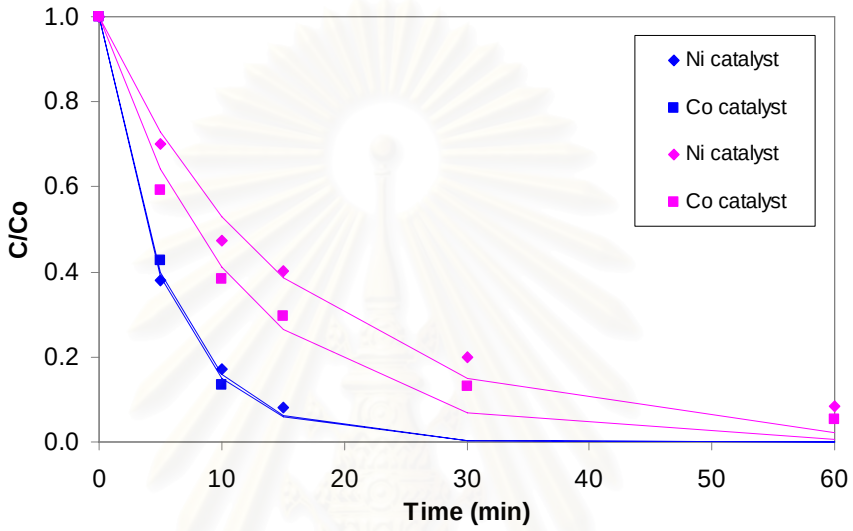

Figure 6.4 Effect of phenol concentration for two metal catalysts in 3-phase FBR (— : 10 ppm and — : 100 ppm of initial phenol concentration)

In **Figure 6.4** the Co-metallic catalyst exhibits comparable efficiency as Ni-metallic catalyst at 10 ppm of initial phenol concentration. As the initial concentration of phenol was raised from 10 to 100 ppm, the efficiency of Co-metallic catalyst was definitely higher than Ni-metallic catalyst. The metal active sites analyzed by gas chemisorption in **Table 6.4** confirm that Co-metallic catalyst has more efficiency. It is because of the more active sites of Co-metallic catalyst.

Table 6.4 Metal active sites of metallic catalyst

Catalyst	Metal active sites ($x10^{-19}$ sites/g catalyst)
5%wt Co/MC	16.3 [a]
5%wt Ni/MC	8.1 [b]

[a] Determined by H_2 pulse chemisorption

[b] Determined by CO pulse chemisorption

The mechanism of the adsorption of phenol on oxide catalysts can be considered in the framework of donor/acceptor interactions in which the catalysts enter in the role of Lewis acids. Consequently, the direction and rate of the oxidation of phenol must depend on the acid/base properties of the catalyst surface. *Kochetkova et al. (1992)* proposed that the catalytic activity of metal oxide catalysts during oxidation of phenol shows the following order: CuO > CoO > Cr_2O_3 > NiO > MnO_2 > Fe_3O_3 > YO_2 > Cd_2O_3 > ZnO > TiO_2 > Bi_2O_3 [36]. By the reasons, it might be concluded that the catalytic activity of Co is higher than Ni catalyst.

6.3.2 Deactivation of cobalt catalyst

The useful life of a catalyst is a critical criterion for the commercialization of the present FBR technology, as the cost of the catalyst is a major factor contributing to the operating costs of the system. The metallic catalysts which have been used until now undergo serious activity losses and deactivations due to the strong oxidation conditions of the processes used.

To investigate the deactivation of Co catalyst on 3-phase FBR, the experiments were performed using the same Co catalyst in the reactor for three consecutive batches (60 min per each batch). The following operating conditions are chosen: 2 L of 100 ppm initial phenol solution with flow rate 1 L/min. As for the catalytic treatment in the 3-phase fluidized bed reactor, we used 5 g catalyst loading and 1 L/min of ozone flow rate.

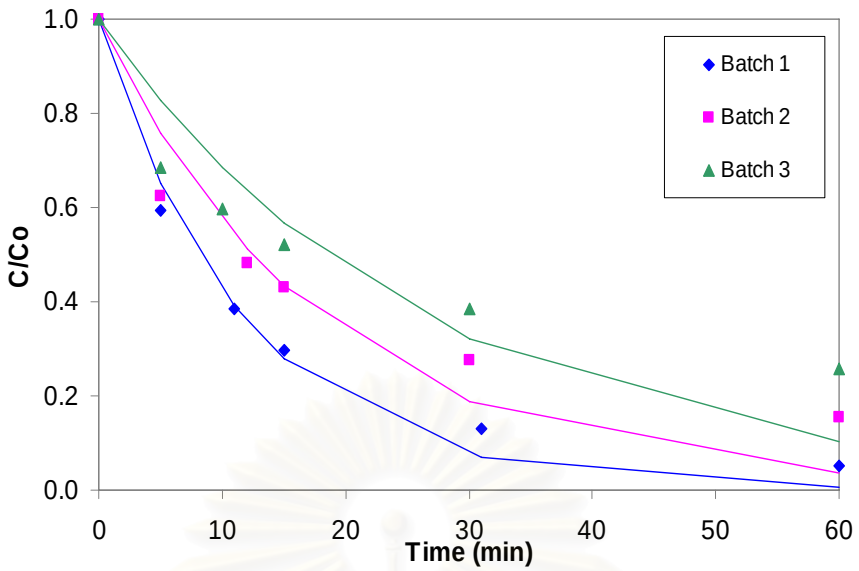

Figure 6.5 Deactivation of Co catalyst on phenol degradation after repeated use in three consecutive runs.

When the experiment was repeated for three batches without changing the catalyst, the efficiency tended to decrease (see **Figure 6.5**). The results suggested that the cobalt catalyst suffered deactivation in the 3-phase FBR. To confirm these results, H_2 chemisorption was used to characterize the active cobalt metal sites on the catalyst.

H_2 chemisorption was carried out following the procedure described by Reuel and Bartholomew using a Micromeritics Pulse Chemisorb 2750 system. Prior to H_2 chemisorption, approximately 0.2 gram of the catalysts were reduced at 350°C after ramping at a rate of 10 ^{o}C min^{-1} and held at that temperature for 3 h. Static H_2 chemisorption was performed at 100 ^{o}C.

Table 6.5 Metal active sites of fresh and spent Co catalyst from H_2 chemisorption

Catalyst	Metal active sites[a] (x10^{-19} sites/g catalyst)	
	Fresh	Spent (after run 3 batch)
Co metallic	16.3	13.9

[a] Error of measurement was ± 5%.

The result of H_2 chemisorption test in **Table 6.5** reveals that the amount of metal active sites after three consecutive batches decrease apparently. This point corresponded to the results from catalytic treatment in 3-phase fluidized bed reactor in **Figure 6.5**. It indicates that there was deactivation of the catalyst and decrease the ability of decomposition down. However, *Arena et al., (2003)* [37] proposed that the cause of catalyst suffer deactivation during the oxidation process is by the leaching of the metal cation. It has been proved that the dissolved metal from the catalyst produces an important reaction extension in the liquid phase changing the heterogeneous catalysis into homogeneous and increases significantly the toxicity of the reactor effluent.

Based on these experiment results we may conclude that it is technically feasible to apply these metallic catalysts to wastewater treatment. However, in our further study we should consider the deactivation of metallic catalyst and the regeneration method.

6.3.3 Investigation of phenol degradation in continuous system

All the experiments before this section were operated in circulated system. As mentioned in the experimental procedure, the entire solution was re-circulated via the hold-up tank until the end of the treatment time. But for the continuous case the system need one more tank, liquid pump and liquid flow meter for adding phenol solution with constant flow rate into the hold-up tank. The entire solution from reactor was drained out all the time with no turn back to the tank (see **Figure 6.6**).

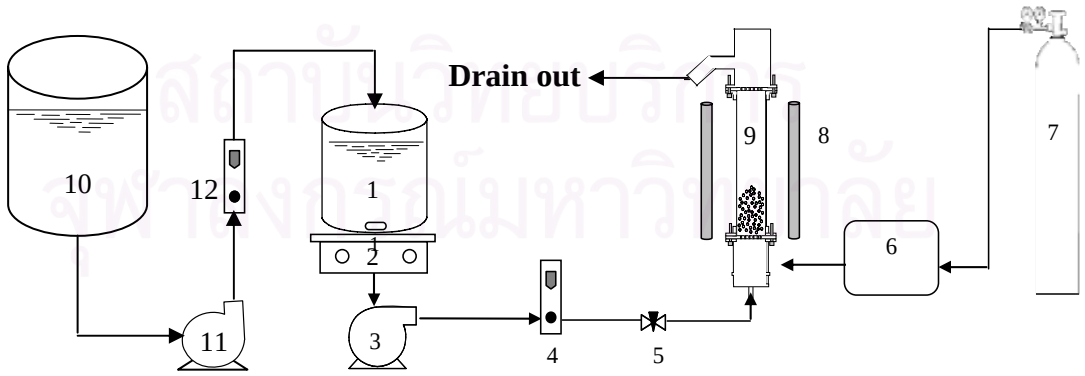

Figure 6.6 Diagram of equipment setup for continuous system;1.hold-up tank (T1), 2.magnetic stirrer, 3 and 11.liquid pump, 4 and 12.flow meter, 5.3-way valve, 6.ozone generator, 7.oxygen tank, 8.UV-lamp, 9.lab-scale 3-phase fluidized bed reactor and 10.add-up tank (T2)

In the first two hours, the system was operated as a circulated system. 2 L of 10 ppm aqueous phenol was decomposed by 5 g of Ni-metallic catalyst with 1 L/min of ozone generated from pure oxygen and liquid flow rate. After that, the system was changed to be a continuous system. The liquid flow rate which via reactor was decreased from 1 to 0.1 L/min and the solution from add-up tank (T2) was filled into the hold-up tank (T1) with the same flow rate.

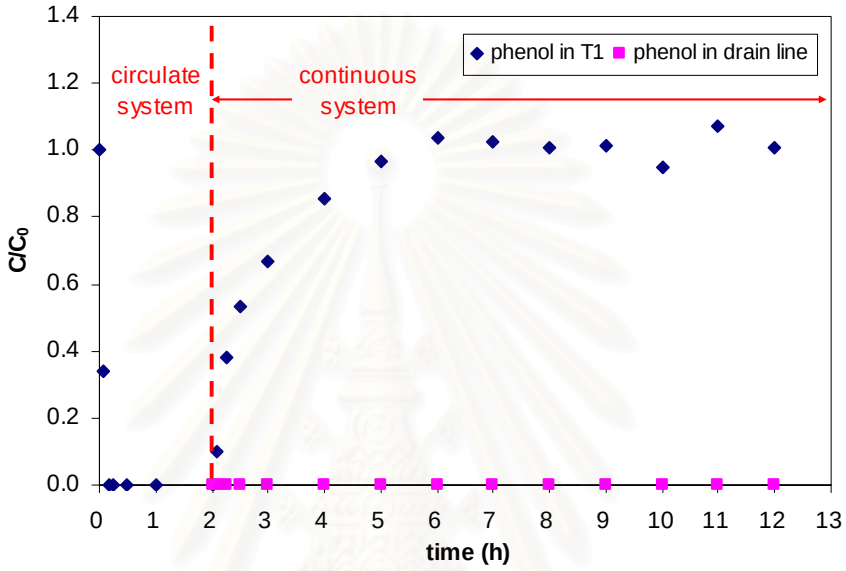

Figure 6.7 Degradation of phenol by 3-phase FBR in continuous system

The result from **Figure 6.7** reveals that phenol was treated within 10 minutes by circulated system. After changing the system, the concentration of phenol started increasing and closed to 10 ppm. But there was no detected phenol in drain line any time. It seems to be possible to treat by continuous system. However, the optimum value of liquid flow rate via reactor is needed to find out. The more flow rate means the more capacity but the resident time in reactor will be decreases. Therefore, it is necessary to find out the proper flow rate with the system.

Besides analyzed by HPLC, TOC analyzer was also used to detect TOC in the solution (see **Figure 6.8**). The result shows that even though phenol and the intermediate product as catechol or hydroquinone is not detected in drain line after treating but TOC still appears at 5-6 ppm. It might be concluded that the treatment is not completely.

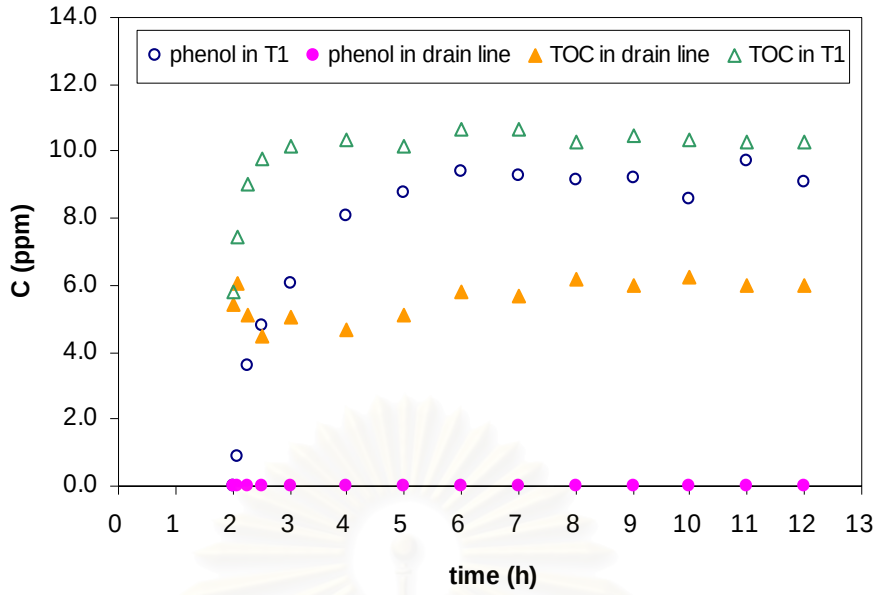

Figure 6.8 TOC concentration of aqueous from drain line and hold-up tank

According to *Matatov et al. (1998)*, the catalytic oxidation process maybe prohibitively expensive when used to achieve the complete oxidation of all organics present to CO_2 and H_2O. As an alternative, the partial oxidation of the organic maybe used to render the wastewater more amenable to other methods of treatment (typically biological) [38].

6.4 Overall comparative catalytic activity

All the experiments in the presence of: only ozone (O_3), only TiO_2 photocatalyst on silica beads, only metal catalyst (Ni or Co) on mesoporous carbon beads, and ozone in combination with one of the mentioned catalysts were carried out under the same operation conditions (2 L of 10 ppm phenol solution, 1 L/min of liquid and/or gas flow rate and 5 g of catalyst loading). For the sake of comparison, phenol concentration change with respect to decomposition time which is obtained from each experiment is plotted in **Figure 6.9**.

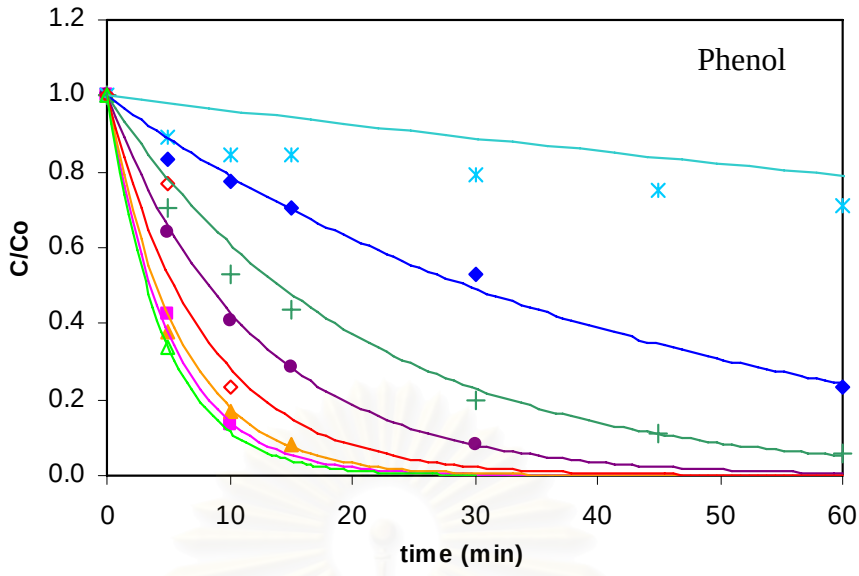

Figure 6.9 Comparison of phenol degradation efficiency in the presence of : only ozone generated from air (♦), only ozone generated from pure oxygen (◊), only TiO_2 12.5 %wt on silica bead (*), only Co 5 %wt on mesoporous carbon bead (•), TiO_2 12.5 %wt on silica bead with ozone generated from air (+), Co 5 %wt with ozone generated from air (■), Ni 5 %wt with ozone generated from air (▲) and Ni 5 %wt with ozone generated from pure oxygen (Δ).

First, we consider the cases of using only ozone or a catalyst. The comparison between metallic catalysts (•) and photocatalyst (*) shows that metallic catalyst was more effective even though the %wt of Co was lower than TiO_2. In addition, comparison between cases of using metallic catalysts (•) and ozone (♦,◊) reveals that the metallic catalyst has a decomposition higher efficiency than that of the ozone generated from air but lower than that of ozone generated from pure oxygen. Obviously using pure oxygen as a gas source will increase the ozone concentrate. Evidently the metallic catalyst is more effective than the photocatalyst. Next the experiments were focused on the case of metallic catalyst together with ozone. The results came out as predicted. Decomposing phenol by metallic catalyst combine with ozone generated from pure oxygen (Δ) gave the best result and was more efficient than the case of ozone generated from air (■,▲). It is noteworthy that in an actual wastewater treatment process it is crucial to minimize the total costs of the treatment system. Therefore the most appropriate case should use the metallic catalyst combined with ozone generated from air.

In addition, the intermediate product (hydroquinone (HQ) and catechol (CC) concentrations are expressed in **Figure 6.10 (a)** and **Figure 6.10 (b)**.

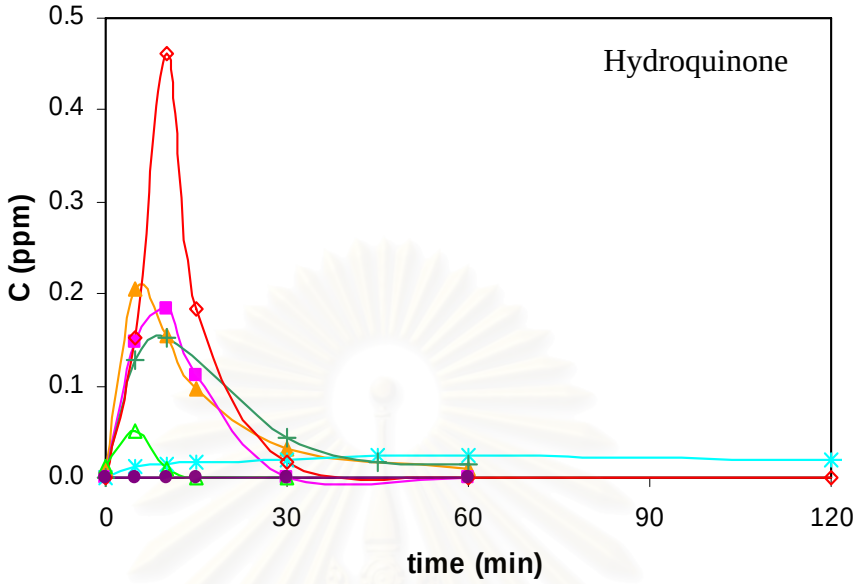

(a)

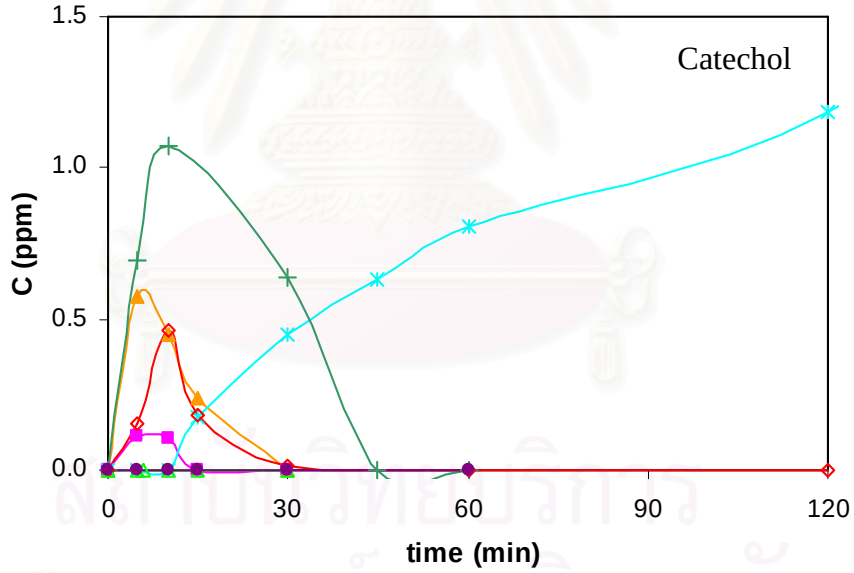

(b)

Figure 6.10 Concentration of hydroquinone (a) and catechol (b) in the presence of : only ozone generated from pure oxygen (◊), only TiO_2 12.5 %wt on silica bead (*), only Co 5 %wt on mesoporous carbon bead (•), TiO_2 12.5 %wt on silica bead with ozone generated from air (+), Co 5 %wt with ozone generated from air (■), Ni 5 %wt with ozone generated from air (▲) and Ni 5 %wt with ozone generated from pure oxygen (Δ)

The results from **Figure 6.10 (a)** show that the hydroquinone in each case was produced in an insignificant amount and it was finally decomposed to a concentration less than 0.5 ppm in 30 min. Meanwhile the production of catechol in **Figure 6.10 (b)** were also minute but still higher than that of hydroquinone. Catechol in every case, except the case of using only TiO_2 12.5 %wt on silica bead, was degraded within 60 min. It is attributed to the fact that with only TiO_2, efficiency of catechol decomposition was very low. Therefore phenol compounds in the solution would be decomposed and transformed to intermediate product in a relatively slow rate.

Zhang et al. (2006) reported the pathways and kinetics on photocatalytic destruction of aqueous phenol and calculated the reaction rate constants of phenol, catechol (CC), hydroquinone (HQ), hydroxyhydroquinone (HHQ), organic acids (OA). The reported rate constants were 0.036, 0.020, 0.014, 0.048, 0.012 mmol/(dm^3.minute), respectively. It was observed that with TiO_2 catalyst phenol tends to be decomposed to catechol [39]. It should be noted that experimental result shown in **Figure 6.10** is also consistent with the experimental results of *Zhang et al.* It could be clearly seen that with TiO_2 photocatalyst, the amount of catechol was higher than that of hydroquinone.

From **Figure 6.9**, it could be clearly observed that when a catalyst of Ni 5 %wt with ozone generated from pure oxygen was employed the lowest concentration of phenol remained in the investigated system. Therefore, it is considered that decomposition of phenol with the catalyst of Ni 5 %wt with ozone generated from pure oxygen is the base case. It is worth to investigate in a further detail on the TOC concentration in the system.

Confirmation by TOC analysis in **Figure 6.11** reveals that it took 10 min for degrading phenol to a concentration less than 1 ppm while TOC in the aqueous solution need longer time (90 min) to be decomposed almost completely. This could be implied that all of the intermediate products would be decomposed completely.

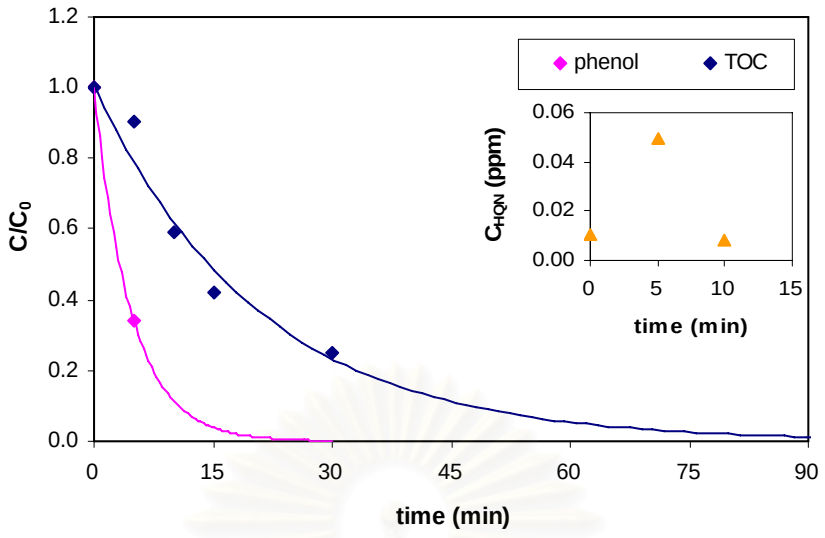

Figure 6.11 TOC concentration in the case of decomposition by 5 g of Ni 5 %wt with ozone generated from pure oxygen

6.5 Possibility of nickel catalyst for phenol degradation in pilot-scale fluidized bed reactor

Based on laboratory-scale experimental results, Ni-metallic catalyst was selected to employ in the pilot-scale three-phase fluidized bed reactor for degrading phenol-polluted wastewater. In order to maintain a fully circulated condition, water from the reactor number 5 (V5) was fed into the tank number 6 (T6), then fed back to the tank number 1 (T1) and circulated continuously through the system (see the schematic flow diagram in chapter V). Three typical experimental conditions employed in batch 3, 4 and 7 are shown in **Table 6.6**, respectively. With respect to the mentioned conditions, samples of contaminated aqueous solution were taken for analyses and then the results were shown in **Figure 6.12**.

Table 6.6 Operating conditions of the pilot-scale fluidized bed reactors

Conditions	Batch 3	Batch 4	Batch 7
Initial phenol concentration (ppm)	19.8	16.8	19.2
Total amount of catalyst (g)	200	200	200
Total liquid volume (L)	720	720	720
Liquid flow rate (L/min)	4	7	7
Gas flow rate (L/min)	5	4	4

In batch 3, ozone with a flow rate of 5 L/min generated from the ozone generator (SO-O3UN-OX, Tokyu Car Co., Ltd) was mixed with 20 L/min of oxygen before being divided equally into 5 reactors. While in batch 4, 5 L/min of ozone from the ozone generator (SO-O3UN-OX) was mixed with 15 L/min of ozone produced by another ozone generator supported by Walailuck University. Finally, in batch 7, 20 L/min of ozone from the newest ozone generator (OZ-7540, Asia-Tech Engineering Co., Ltd) was employed to decompose the aqueous solution with the same phenol concentration. It is noted that all the ozone in every batch was generated from pure oxygen.

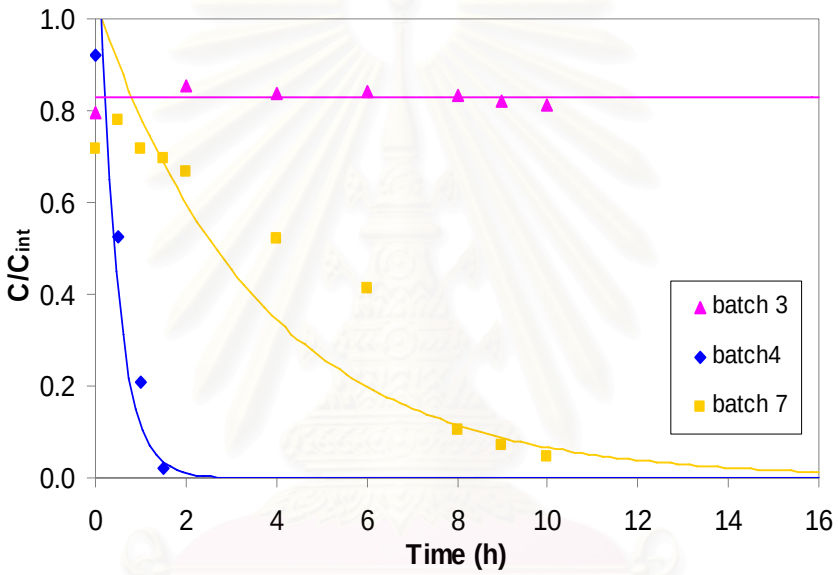

Figure 6.12 Decomposition efficiency of phenol compared between batches 3, 4 and 7

In batch 3, after operating for 10 hours only 20 % of phenol was decomposed. This unsatisfactory result was attributed to an inadequate amount of ozone fed into the system. To improve the efficiency, capacity of ozone generator to supply to the system should be increase.

In batch 4, to verify the above conclusion, another ozone generator supported by Walailuck University was added to convert oxygen gas to ozone for supplying into the system. 15 L/min of ozone produced from the second ozone generator was mixed with 5 L/min from the first generator (SO-O3UN-OX). It was found that much higher amount of phenol decomposition in batch 4 was decomposed in comparison with that of batch 3. It spent only about 2 hours to decompose phenol to a concentration of less than 1 ppm (see **Table 6.7**).

Table 6.7 Decomposition efficiency of phenol in batch 4

Time	C/C_{int}										
(h)	T1	V1	T2	V2	T3	V3	T4	V4	T5	V5	T6
0	0.75	0.65	0.68	0.64	0.66	0.72	0.74	0.81	0.74	0.99	0.92
0.5	0.67	0.72	0.69	0.54	0.54	0.40	0.45	0.40	0.42	0.33	0.53
1	0.33	0.33	0.41	0.28	0.34	0.17	0.15	N/D	0.19	0.11	0.21
1.5	0.25	0.17	0.18	0.12	0.14	0.09	0.11	0.03	0.04	N/D	0.02
2	0.08	N/D	N/D	N/D	N/D	N/D	N/D	N/D	N/D	N/D	N/D

Remark : N/D = Non-Detectable

After further treatment the color of the wastewater changed from transparent to yellowish and brownish. This color changing is attributed to formation of unidentified intermediate products. These products could also lead to the catalyst deactivation by attaching or coating on the catalysts and decreased the effective surface area (please refer to the results in the section 6.3.2 Deactivation of cobalt catalyst on lab-scale took place in 3 phase fluidized bed reactor).

To prove this postulation that the catalysts were deactivated by the intermediate products we set up a simple experiment in batch 6 in which regenerating of the catalysts was not conducted by reducing the number of the reactors down (reducing the total liquid volume to 80 L and running the circulated system through just one reactor) but still maintained the flow rates of the liquid and gas streams. Comparison of the results of batch 6 and 4 reveals that phenol in batch 6 would be degraded just 30 % after 10 hours passed while in the batch 4 almost all phenol was degraded in 2 hours. It confirmed that the catalysts were certainly deactivated. Therefore, the catalysts need to be regenerated before starting the next batch. A new ozone generator which has more capacity was ordered and bought from Asia-Tech Engineering Co., Ltd. With a new ozone generator the catalysts were regenerated by flowing tap water at 4 L/min of ozone per each reactor through the system for 6 hours.

After that the experiment in batch 7 was set up by using the same liquid and gas flow rate as batch 4. All ozone was produced by only new ozone generator model OZ-7540. It was found that nearly all of the phenol was degraded in 10-12 hours (see **Table 6.8**).

Table 6.8 Decomposition efficiency of phenol in batch 7

Time	C/C_{int}										
(h)	T1	V1	T2	V2	T3	V3	T4	V4	T5	V5	T6
0	0.78	0.81	0.82	0.81	0.84	0.83	0.95	0.80	0.82	0.72	0.72
2	0.69	0.67	0.71	0.66	0.69	0.60	0.65	0.64	0.68	0.66	0.67
4	0.56	0.49	0.55	0.51	0.50	0.49	0.52	0.51	0.54	0.48	0.52
6	0.43	0.43	0.42	0.42	0.42	0.41	0.47	0.40	0.46	0.41	0.41
8	0.13	0.12	0.13	0.12	0.12	0.12	0.13	0.10	0.12	0.10	0.10
9	0.09	0.07	0.09	0.06	0.08	0.06	0.08	N/D	N/D	0.04	0.07
10	N/D	N/D	N/D	N/D	N/D	N/D	N/D	N/D	0.05	N/D	0.05
12	N/D	N/D	N/D	N/D	N/D	N/D	N/D	N/D	N/D	N/D	N/D
14	N/D	N/D	N/D	N/D	N/D	N/D	N/D	N/D	N/D	N/D	N/D
16	N/D	N/D	N/D	N/D	N/D	N/D	N/D	N/D	N/D	N/D	N/D

In addition after operating for 16 hours the color of the wastewater changed to be transparent again (see **Figure 6.13)**.

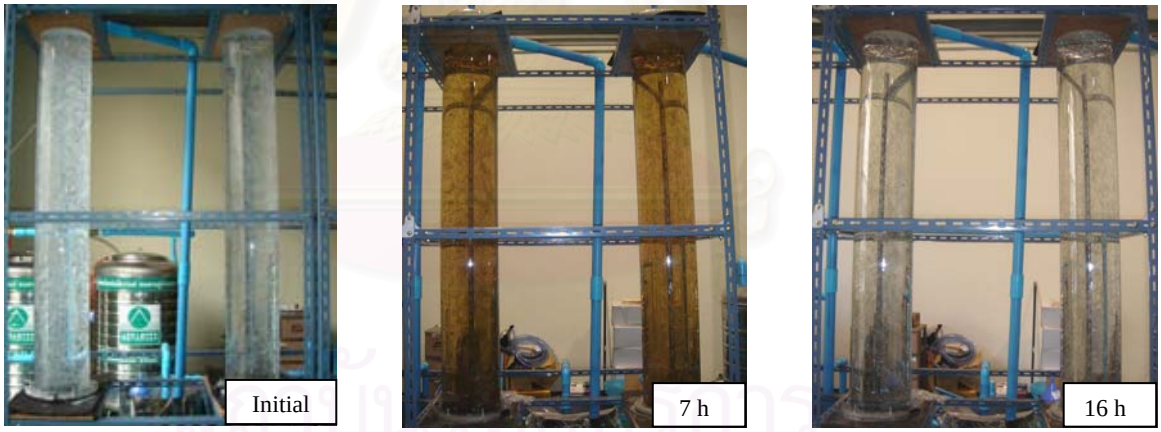

Figure 6.13 Color of the solution at the initial and after treated for 7 and 16 h.

From the changing of the wastewater color of it is reasonable to that the intermediate products have been degraded finally. In **Figure 6.14**, we considered that the peak found at the retention time 1.8~1.9 min of HPLC chromatogram was an intermediate product that produced yellow color. To confirm that the intermediate product would disappear at 16 h, the HPLC chromatogram for the effluent stream of the last reactor V5 was analyzed and it was found that there was no detectable peak left at retention time of 1.8~1.9 min.

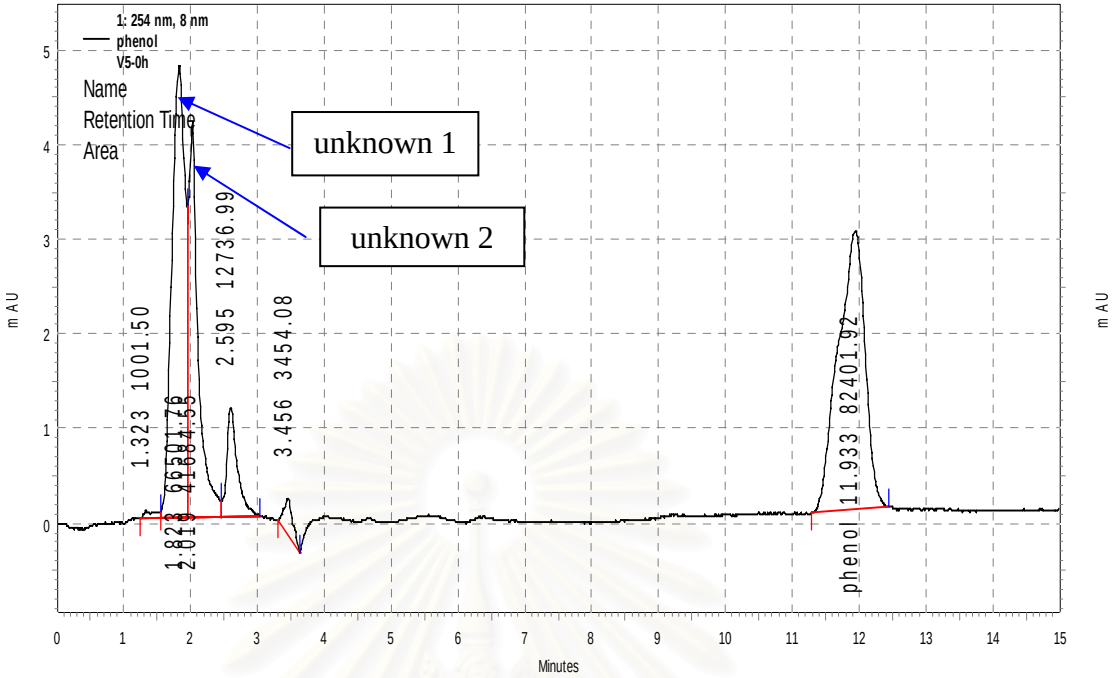

(a) HPLC chromatogram at 0 h (reactor V5)

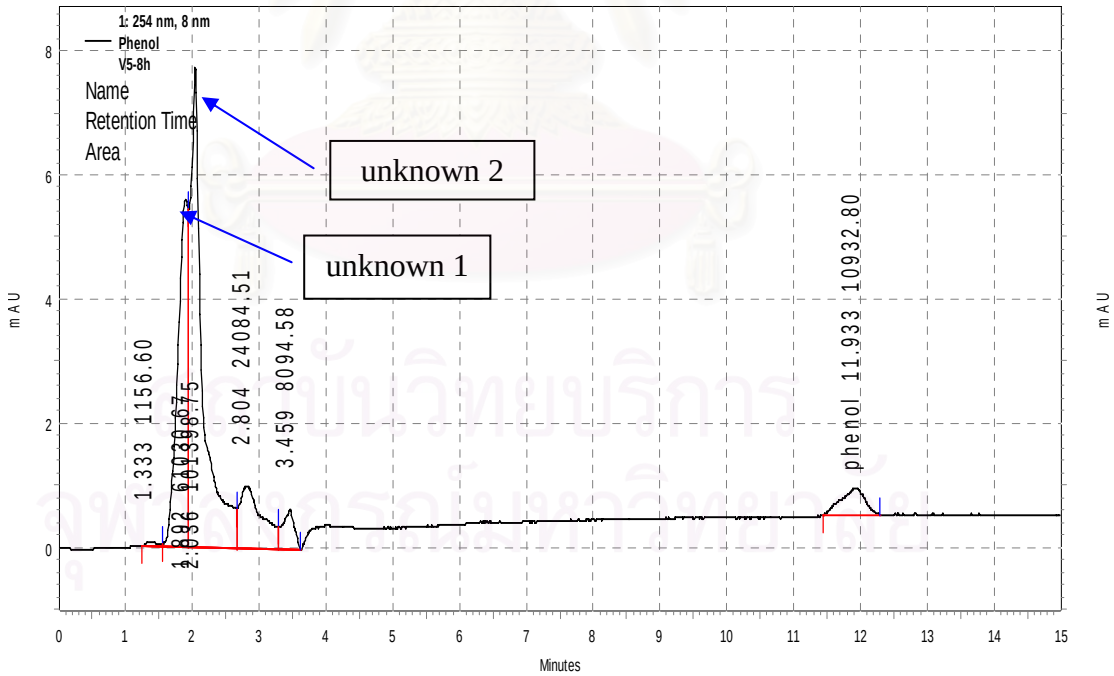

(b) HPLC chromatogram at 8 h (reactor V5)

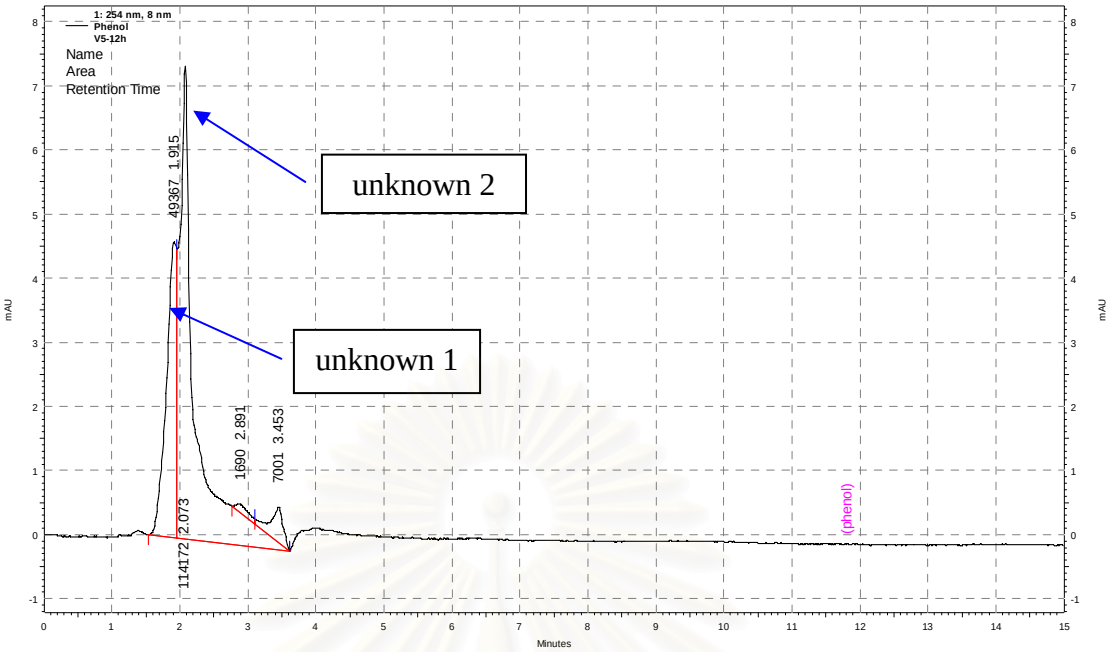

(d) HPLC chromatogram at 12 h (reactor V5)

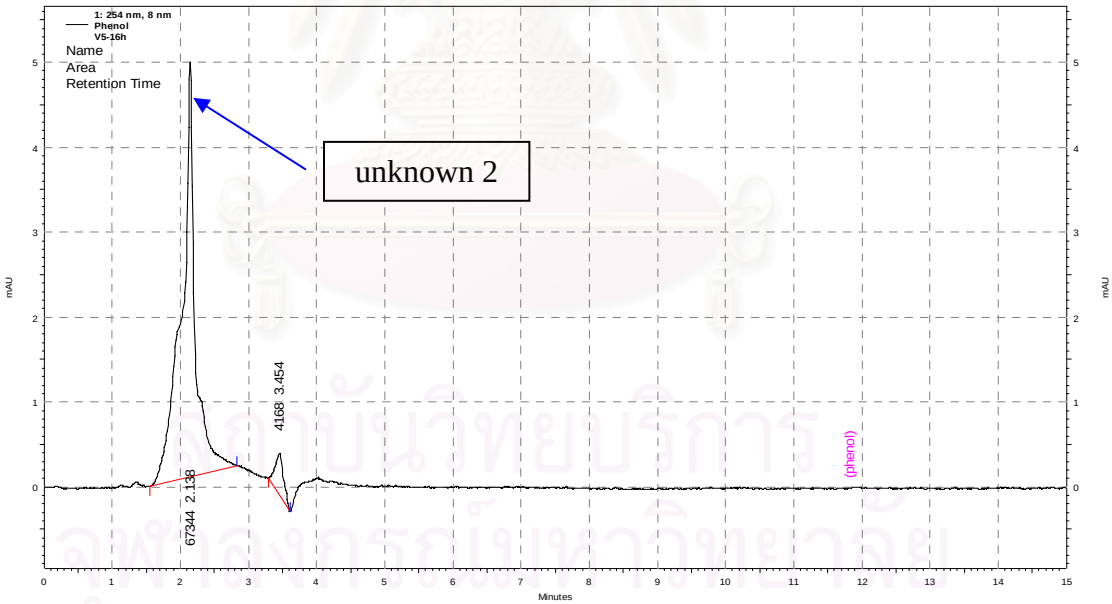

(e) HPLC chromatogram at 16 h (reactor V5)

Figure 6.14 HPLC chromatogram of phenol and intermediate products of the solution in reactor number 5 V5) at 0, 8, 12 and 16 h.

CHAPTER VII

CONCLUSIONS AND RECOMMENDATIONS

Conclusions and recommendations for future research are presented in this chapter.

7.1 Conclusions

The conclusions of this research are summarized as follows :

1. There is an optimum amount of catalyst loaded into the fluidized bed reactor, which could provide the best decomposition performance.

2. The photocatalyst had a lower degradation performance than the metal catalyst. Moreover, the electrical energy for UV-C lamps further increased the operating cost.

3. The cobalt metallic catalyst is more efficient than the nickel catalyst, though the nickel metallic catalyst is more economical.

4. Applying the metallic catalyst with ozone generated from pure oxygen gives the best results. However, using air instead of pure oxygen can save more costs whereas the total efficiency differs insignificantly.

7.2 Recommendations for future studies

From the previous conclusions, the following recommendations for future studies are proposed.

1. To apply these metallic catalysts to a wastewater treatment system, an effective regeneration method of the metallic catalysts is an issue to be investigated further.

2. There are some fine powders detaching from the carbon support after testing for a while. Therefore an improvement of these metallic catalysts stability is needed.

3. The system in the section of dissolving ozone into the water should be improved, for instance, by adapting static mixer unit, to increase the solubility of ozone.

REFERENCES

1. J. H. Lee, W. Nam, M. Kang, G. Y. Han, K. J. Yoon,M. Kim, K. Ogino, S. Miyata, S. Choung. Design of two types of fluidized photo reactors and their photocatalytic performances for degradation of methyl orange. Applied Catalysis A: General, 244, (2003) : 49–57
2. T. Keiichi*, A.Keiji and H. Teruaki. Photocatlytic water treatment on immobilized TiO2 combined with ozonation. Journal of Photochemistry and Photobiology A: Chemistry, 101 (1996) : 85-87
3. A. J. Feitz B. H.. Evaluation of two solar pilot scale fixed-bed photocatalytic reactors. Water Research, Vol. 34, No. 16 : 3927-3932
4. M. F. J. Dijkstra, H. Buwalda, A. W. F. de Jong, A. Michorius, J. G. M. Winkelman, A. A. C. M. Beenackers. Experimental comparison of three reactor designs for photocatalytic water purification. Chemical Engineering Science, 56 (2001) : 547-555
5. L. Zhang, T. Kanki, N. Sano, A. Toyoda. Development of TiO_2 photocatalyst reaction for water purification. Separation and Purification Technology, 31 (2003) : 105-110
6. K. Nakano, E. Obuchi, S. Takagi, R. Yamamoto, T. Tanizaki, M. Taketomi, M. Eguchi, K. Ichida, M. Suzuki and A. Hashimoto. Photocatalytic treatment of water containing dinitrophenol and city water over TiO_2/SiO_2. Separation and Purification Technology, 34 (2004) : 67-72
7. A. A. C. Magalhães, D. L. Nunes, P. A. Robles-Dutenhefner, E. M. B. de sousa. Catalytic activity of porous TiO2 obtained by sol-gel process in the degradation of phenol. Journal of Non-crystalline Solids, 348 (2004) : 185-189
8. C.M. Ling. Performance of the photocatalytic reactors using immobilized TiO_2 film for the degradation of phenol and methylene blue dye present in water stream. Chemosphere, 57 (2004) : 547-554
9. T. Kanki, S. Hamasaki, N. Sano, A. Toyoda and K. Hirano. Water purification in a fluidized bed photocatalytic reactor using TiO_2-coated ceramic particles. Chemical Engineering Journal, 108 (2005) : 155–160

10. S. Atul, N. Hiroyuki and M. Kouichi*. A novel nickel/carbon catalyst for CH4 and H_2 production from organic compounds dissolved in wastewater by catalytic hydrothermal gasification. Fuel, 85 (2006) : 179-184

11. Agency for Toxic substances and Disease registry (ATSDR) 1998, Toxicological profile for phenol, ATSDRIC@cdc.gov

12. William M. Throop. Alternative methods of phenol wastewater control. Journal of Hazardous Materials, 1 (1975/77) : 319-329

13. P. Kari* and S. Mika. Heterogeneous water phase catalysis as an environmental application: a review. Chemosphere, 48 (2002) : 1047-1060

14. A. Alejandre, F. Medina, A. Fortuny, P. Salagre, J.E. Sueiras. Characterisation of copper catalysts and activity for the oxidation of phenol aqueous solutions. Applied Catalysis B: Environmental 16 (1998) : 53-67

15. St.G. Christoskova, M. Stoyanova, M. Georgieva. Low-temperature iron-modified cobalt oxide system Part 2. Catalytic oxidation of phenol in aqueous phase. Applied Catalysis A: General 208 (2001) : 243–249

16. H. Joglekar, S. Samant, J. Joshi. Kinetics of wet air oxidation of phenol and substituted phenols. Water Res, 25 (1991) : 135

17. K. Kavita, C. Rubina* and Rameshwar L. Sawhney. Treatment of hazardous organic and inorganic compounds through aqueous-phase photocatalysis: A review. Ind. Eng. Chem. Res., 43 (2004) : 7683-7696

18. A. Mills and S. Le Hunte. An overview of semiconductor photocatalysis. Journal of Photochem Photobiol A: Chem, (1997) : 108

19. O. Carp, C.L. Huisman and A. Reller. Photoinduced reactivity of titanium dioxide. Progress in Solid State Chemistry, 32 (2004) : 33–177

20. M. Sameiro T. Goncçalves, Elisa M.S. Pinto, P. Nkeonye, Ana M.F. Oliveira-Campos. Degradation of C.I. Reactive Orange 4 and its simulated dyebath wastewater by heterogeneous photocatalysis. Dyes and Pigments, 64 (2005) : 135-139

21. A. Sobczyński, Ł. Duczmal, W. Zmudziński. Phenol destruction by photocatalysis on TiO_2: an attempt to solve the reaction mechanism. Journal of Molecular Catalysis A: Chemical, 213 (2004) : 225–230

22. C.-R. Huang and H.-Y. Shu. The reaction kinetics, decomposition pathways and intermediate formations of phenol in ozonation, UV/O_3 and UV/H_2O_2 processes. Journal of Hazardous Materials, 41 (1995) : 47-64

23. M. Dore, B. Langlais, B. Legube. Ozonation des phenols et des acides phenoxyacetiques. Water Research, Vol. 12 (1978) : 413 – 425

24. S. Esplugas, J. Gim!enez, S. Contreras, E.Pascual, M. Rodríguez. Comparison of different advanced oxidation processes for phenol degradation. Water Research, 36 (2002) : 1034–1042

25. S. Guittoneau, J. De Laat, JP Duguet, C. Bonnel, M. Dore. Oxidation of parachloronitrobenzene in dilute aqueous solution by O_3+UV and H_2O_2+UV: a comparative study. Ozone Sci Eng, 12 (1990) : 73–94

26. F. J. Beltrán, J. M. Encinar, M. A Alonso. Nitroaromatic hydrocarbon ozonation in water. 2. Combined ozonation with hydrogen peroxide or UV radiation. Ind Eng Chem Res, 37 (1998) : 32–40

27. J. Chen, L. Eberlein, Cooper H. Langford. Pathways of phenol and benzene photooxidation using TiO_2 supported on a zeolite. Journal of Photochemistry and Photobiology A: Chemistry,148 (2002) : 183–189

28. D. Duprez, J. Delanoë, J. Barbier Jr., P. Isnard, G. Blanchard. Catalytic oxidation of organic compounds in aqueous media. Catal. Today, 29 (1996) : 317

29. L. S. Fan. Gas-Liquid-Solid Fluidization Engineering. New York : Butterworths Publishers, 1989

30. V. V. Kelkar, K. M. Ng. Development of Fluidized Catalytic Reactors: Screening and Scale-up. AIChE Journal, Vol.48, No. 7 (2002) : 1498-1518

31. J. C. Smith, P. Harriott, W. McCabe. Unit operation of chemical engineering (5th Edition), McGraw-Hill, 1993

32. J. Jansson, A.E.C. Palmqvist, E. Fridell, M. Skoglundh, L. Österlund, P. Thormählen, V. Langer. On the Catalytic Activity of Co_3O_4 in Low-Temperature CO Oxidation. Catal. 211 (2002) : 387–397

33. G. Zhoua, Y. Jiang, H. Xie, Fali Qiu . Non-noble metal catalyst for carbon monoxide selective oxidation in excess hydrogen. Chemical Engineering Journal,109 (2005) : 141–145

34. M. R. Hofmann, S. T. Martin, W. Choi, D. W. Bahnemann. Environmental applications of semiconductor photocatalysis. Chem. Rev. 95 (1995) : 69–96

35. D. Chen, A. K Ray. Photodegradation kinetics of 4-nitrophenol in TiO_2 suspension. Water Res. (1998), 32 (11) : 3223

36. R. P. Kochetkova, A. F. Babikov, L. I. Shiplevskaya, I. P. Shiverskaya, S.A. Eppel, F. K. Smidt. Liquid-Phase Oxidation of Phenol. Khim. Tekhnol. Topl. Masel (1992a), 4, 31 ; *Chem. Abstr.* (1992), 117, 156952

37. F. Arena, R. Giovenco, T. Torre, A. Venuto, A. Parmaliana. Activity andresistance to leaching of Cu-basedcatalysts in the wet oxidation of phenol. Applied Catalysis B: Environmental, 45 (2003) : 51–62

38. Y. I. Matatov-Meytal and M. Sheintuch. REVIEWS Catalytic Abatement of Water Pollutants. Ind. Eng. Chem. Res., 37 (1998) : 309-326

39. L. Zhang, T. Kanki, N. Sano and A. Toyoda. Pathways and kinetics on photocatalytic destruction of aqueous phenol. Environmental Monitoring and Assessment, 115 (2006) : 395–403

APPENDICES

APPENDIX A

CALCULATION OF THE CRYSTALLITE SIZE

Calculation of the crystallite size by Debye-Scherrer equation

The crystallite size calculated from the half-height width of the diffraction peak of XRD pattern using the Debye-Scherrer equation.

From Scherrer equation:

$$D = \frac{K\lambda}{\beta \cos\theta} \tag{A.1}$$

where D = Crystallite size, Å

K = Crystallite-shape factor = 0.9

λ = X-ray wavelength, 1.5418 Å for CuKα

θ = Observed peak angle, degree

β = X-ray diffraction broadening, radian

The X-ray diffraction broadening (β) is the pure width of a powder diffraction free from all broadening due to the experimental equipment. α-Alumina is used as a standard sample to observe the experimental broadening since its crystallite size is larger than 2000 Å. The X-ray diffraction broadening (β) can be obtained by using Warren's formula.

From Warren's formula:

$$\beta = \sqrt{B_M^2 - B_S^2} \tag{A.2}$$

where B_M = The measured peak width in radians at half height.

B_S = The corresponding width of the standard material.

Example: Calculation of the crystallite size of Ni/AC catalyst

The half-height width of peak = 2.85^{o} (from Figure A.1)

= $(2\pi \times 2.85)/360$

= 0.04977 radian

The corresponding half-height width of peak of of α-alumina (from the B_S value at the 2 theta of 43.88^{o} in Figure A.2) = 0.00441 radian

The pure width, $\beta = \sqrt{B_M^2 - B_S^2}$

$= \sqrt{0.04977^2 - 0.00441^2}$

= 0.04957 radian

B = 0.04957 radian

2θ = 43.88

θ = 21.94

λ = 1.5418 Å

The crystallite size $= \dfrac{0.9 \times 1.5418}{0.04957 \cos 21.94}$ = 30.04 Å = 3.0 nm

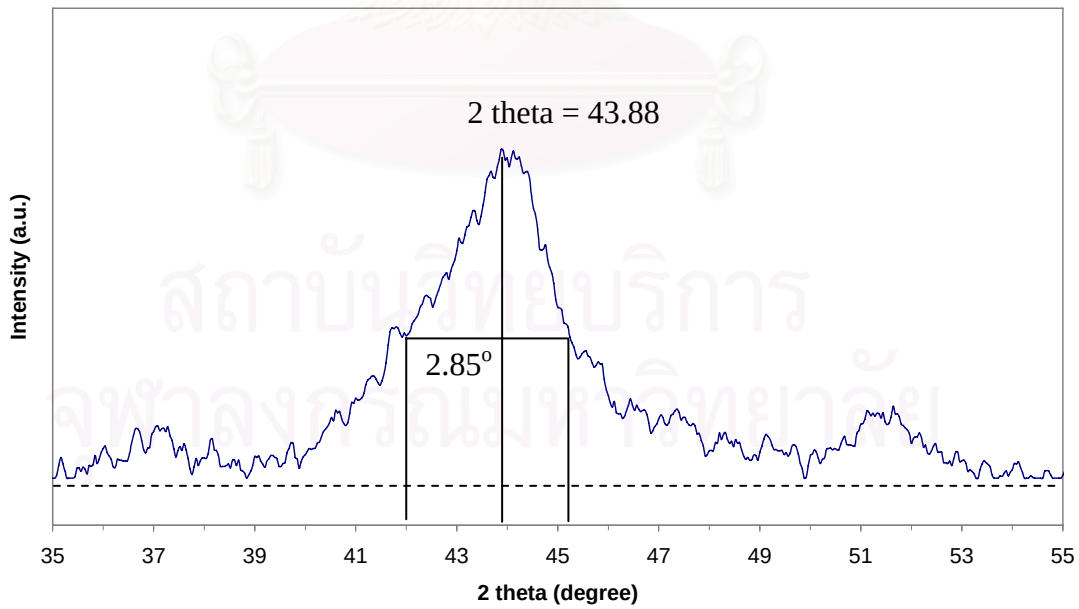

Figure A.1 The observation peak of Ni/AC catalyst for calculating the crystallite size.

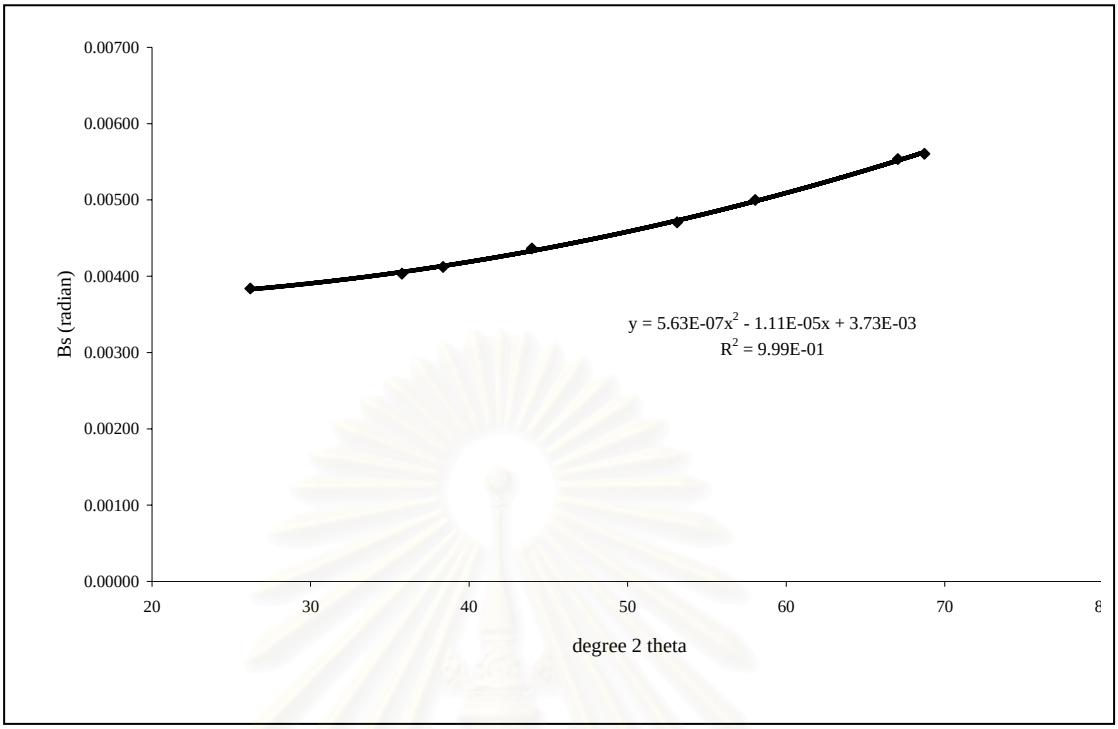

Figure A.2 The graph indicating that value of the line broadening attribute to the experimental equipment from the α-alumina standard.

APPENDIX B

CALCULATION FOR METAL ACTIVE SITES

Calculation of the metal active sites of the nickel catalyst measured by CO adsorption is as follows:

Let the weight of catalyst used	= W	g
Integral area of CO peak after adsorption	= A	unit
Integral area of 45 μl of standard CO peak	= B	unit
Amounts of CO adsorbed on catalyst	= B-A	unit
Volume of CO adsorbed on catalyst	= 45×[(B-A)/B]	μl
Volume of 1 mole of CO at 30°C	= 24.31×10^{6}	μl

Mole of CO adsorbed on catalyst = $[(B-A)/B]\times[45/24.31\times10^{6}]$ mole

Molecule of CO adsorbed on catalyst = $[1.61\times10^{-6}]\times[6.02\times10^{23}]\times[(B-A)/B]$ molecules

Metal active sites = $9.68\times10^{17}\times[(B-A)/B]\times[1/W]$ molecules of CO/g of catalyst

Calculation of the metal active sites of the cobalt catalyst measured by H_2 adsorption is as follows:

Let the weight of catalyst used	= W	g
Integral area of H_2 peak after adsorption	= A	unit
Integral area of 45 μl of standard H_2 peak	= B	unit
Amounts of H_2 adsorbed on catalyst	= B-A	unit
Volume of H_2 adsorbed on catalyst	= 45×[(B-A)/B]	μl
Volume of 1 mole of H_2 at 100°C	= 29.93×10^{6}	μl

Mole of H_2 adsorbed on catalyst = $[(B-A)/B]\times[45/29.93\times10^{6}]$ mole

Molecule of H_2 adsorbed on catalyst = $[1.61\times10^{-6}]\times[6.02\times10^{23}]\times[(B-A)/B]$ molecules

Metal active sites = $9.68\times10^{17}\times[(B-A)/B]\times[1/W]$ molecules of H_2/g of catalyst

APPENDIX C

CALCULATION OF THE HYDRODYNAMICS

In chapter IV, there are mentioned about the hydrodynamic of three-phase fluidized bed reactor. According to the relations in chapter IV, minimum fluidization velocity was preliminary calculated by using the physical properties which measured in this work. These properties and results from calculation are shown in below table.

Table C.1 Hydrodynamics data of lab-scale experiment

Lab-scale

Properties	symbol	Value	SI unit	Remark
Density of liquid	r_L	1000	kg/m^3	
Viscousity of liquid	m_L	0.001	kg/m.s	
Density of wet particle	r_S	1330	kg/m^3	
Diameter of particle	d_p	0.0006	m	
Density of ozone	r_G	1.2	kg/m^3	
Gravitional acceleration	g	9.8	m/s	
Flow rate of gas	F_G	0.000017	m^3/s	1 L/min
Flow rate of liquid	F_L	0.000017	m^3/s	1 L/min
Diameter of reactor	D_R	0.0316	m	
Cross section area of reactor	A_R	0.000784	m^2	

Calculation	symbol	Value	SI unit
Superficial gas velocity	U_G	0.02126	m/s
Superficial liquid velocity	U_L	0.02126	m/s
Archimedes number	Ar	698.544	-
Minimum fluidization velocity of liquid	$U_{mf,LS}$	0.00070	m/s
Minimum fluidization velocity	U_{mf}	0.000424	m/s

Table C.2 Hydrodynamics data of pilot-scale experiment

Pilot-scale

Properties	symbol	Value	SI unit	Remark
Density of liquid	r_L	1000	kg/m^3	
Viscousity of liquid	m_L	0.001	kg/m.s	
Density of wet particle	r_S	1330	kg/m^3	
Diameter of particle	d_p	0.0006	m	
Density of ozone	r_G	1.2	kg/m^3	
Gravitional acceleration	g	9.8	m/s	
Flow rate of gas	F_G	0.000067	m^3/s	4 L/min
Flow rate of liquid	F_L	0.000117	m^3/s	7 L/min
Diameter of reactor	D_R	0.2	m	
Cross section area of reactor	A_R	0.031400	m^2	

Calculation	symbol	Value	SI unit
Superficial gas velocity	U_G	0.00212	m/s
Superficial liquid velocity	U_L	0.00372	m/s
Archimedes number	Ar	698.544	-
Minimum fluidization velocity of liquid	$U_{mf,LS}$	0.00070	m/s
Minimum fluidization velocity	U_{mf}	0.00057	m/s

APPENDIX D

CALIBRATION CURVE FOR HPLC

Phenol

Table D.1 The peak area data of phenol from HPLC

Concentration (ppm)	Peak area
20	122487
40	242991
60	358838
80	472311
100	593542

Cal range: 0 – 100 ppm

Method: 75% water / 25% acitonitrile at 254 nm UV-Vis

Linear fit: C (ppm) = a(Peak area) + b

a = 0.000168134

b = 0

Goodness of fit: r^2 = 0.999604

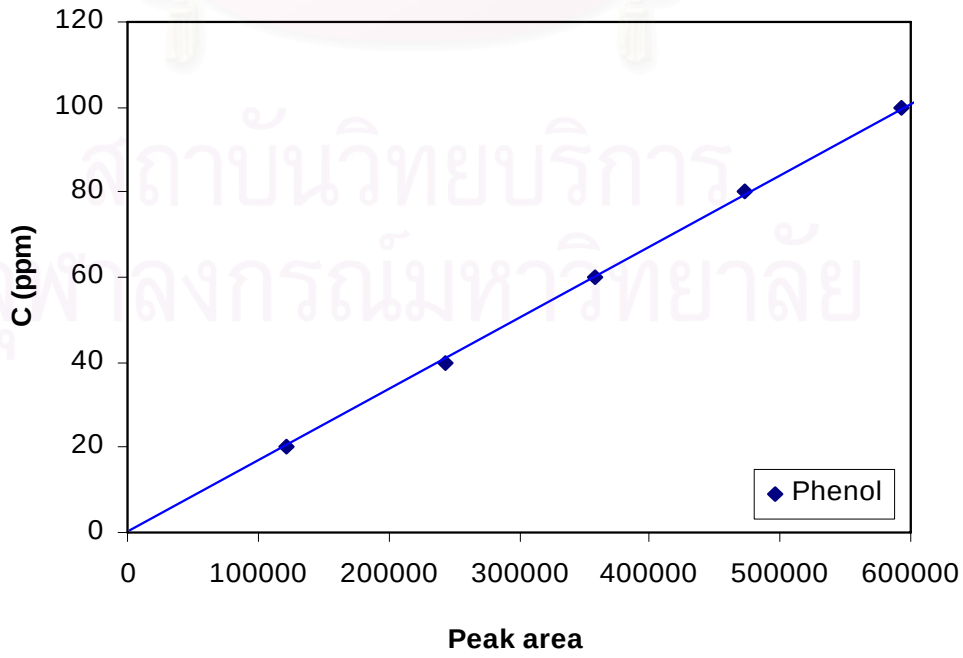

Figure D.1 The calibration curve of phenol

Catechol

Table D.2 The peak area data of catechol from HPLC

Concentration (ppm)	Peak area
20	108164
40	225806
60	311786
80	441430
100	512494

Cal range: 0 – 100 ppm

Method: 75% water / 25% acitonitrile at 254 nm UV-Vis

Linear fit: C (ppm) = a(Peak area) + b

a = 0.000188637

b = 0

Goodness of fit: r^2 = 0.992487

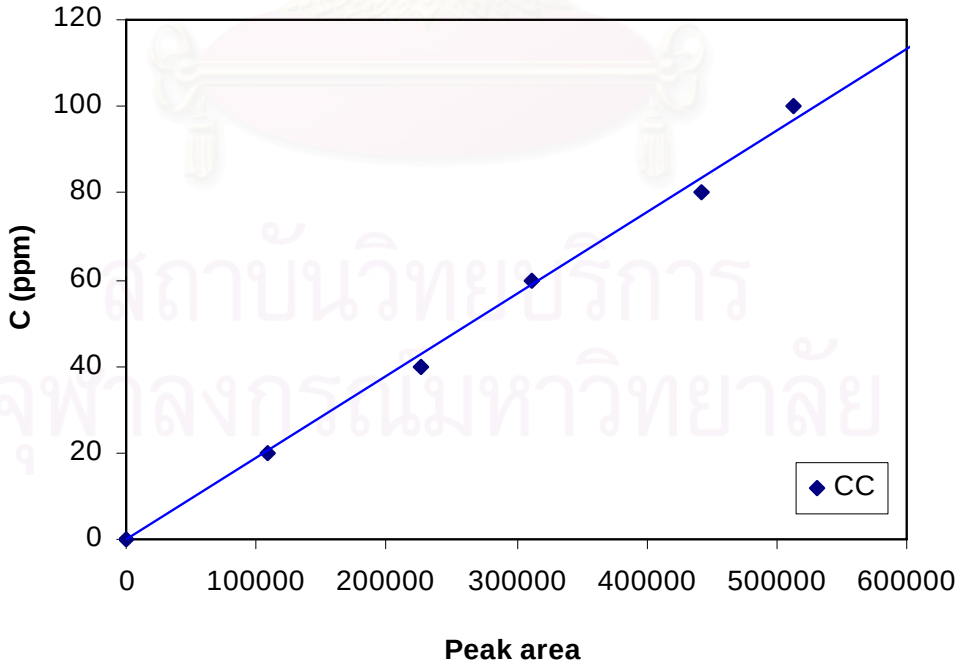

Figure D.2 The calibration curve of catechol

Hydroquinone

Table D.3 The peak area data of hydroquinone from HPLC

Concentration (ppm)	Peak area
20	1106647
40	1753959
60	2145577
80	2518847
100	2816130

Cal range: 0 – 100 ppm

Method: 75% water / 25% acitonitrile at 254 nm UV-Vis

Quadratic fit: $C\ (ppm) = a(\text{Peak area})^2 + b(\text{Peak area}) + c$

$a = 1.09098e^{-11}$

$b = 4.51827e^{-6}$

$c = 0$

Goodness of fit: $r^2 = 0.998541$

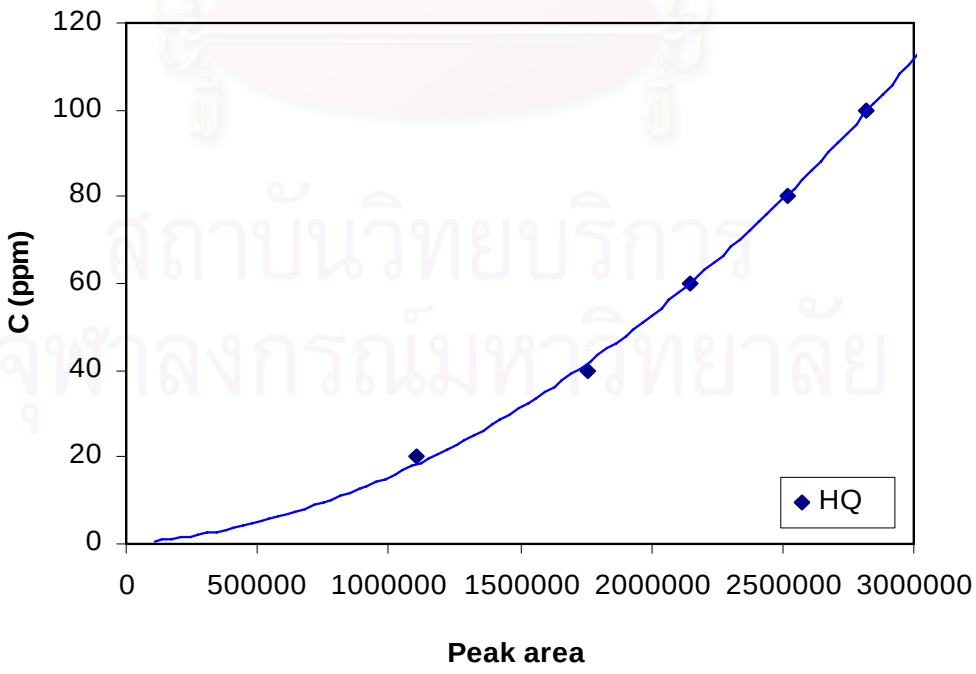

Figure D.3 The calibration curve of hydroquinone

APPENDIX E

RATE CONSTANT

In this appendix, the efficiency for decomposing of 2 L of 10 ppm phenol solution with catalyst loading 5 g was revealed in term of $-\ln(C/C_0)$ to express the rate constant (*k*). The disappearance of phenol followed pseudo first order kinetics. Initial rate constants were determined from the slope of $-\ln(C/C_0)$ vs t (min) plots (**Figure E.1** and **Table E.1**.), where C_0 and C are the phenol concentration at zero time and time t, respectively.

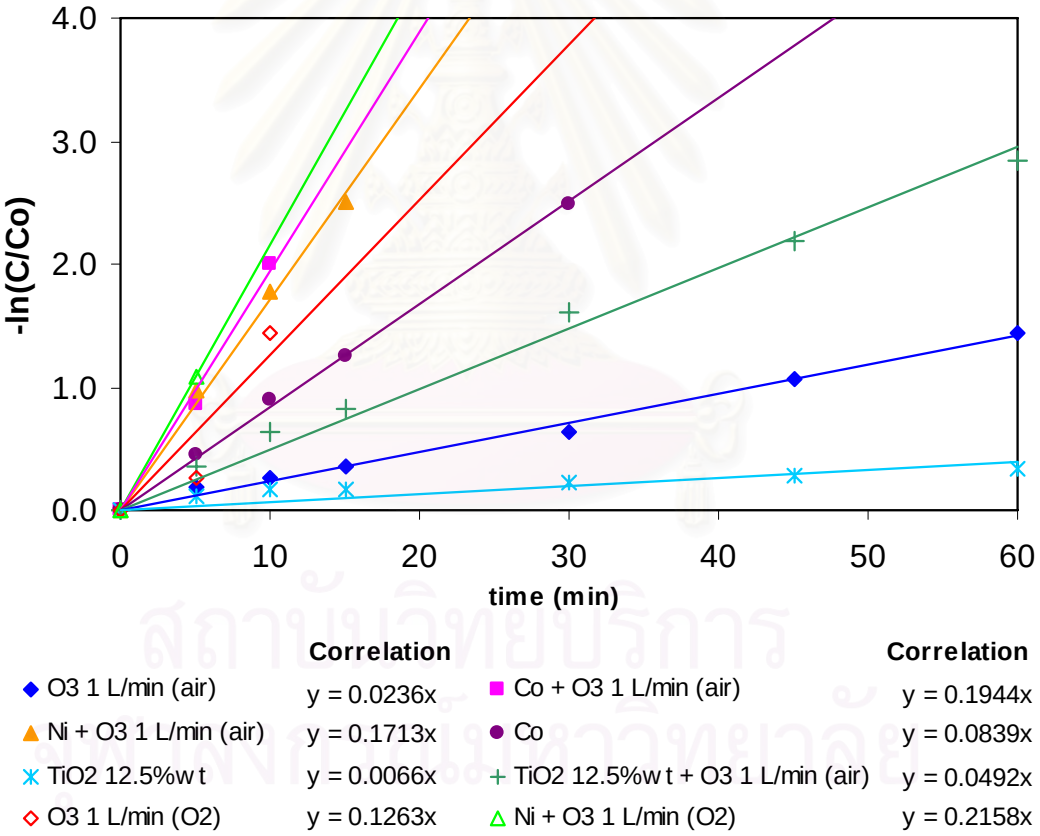

Figure E.1 Phenol decomposition rates.

Table E.1 Pseudo first order rate constant for decomposition of aqueous phenol

Condition	**R^{2a}**	**k (min^{-1})[b]**
Ni + O_3 1 L/min (O_2)	0.9993	0.2158
Ni + O_3 1 L/min (air)	0.9943	0.1713
Co + O_3 1L/min (air)	0.9911	0.1944
O_3 1 L/min (O_2)	0.8583	0.1263
Co	0.9984	0.0839
TiO_2 12.5%wt + O_3 1L/min (air)	0.9893	0.0492
O_3 1 L/min (air)	0.9938	0.0236
TiO_2 12.5%wt	0.6722	0.0066

[a] Correlation coefficient of the straight line

[b] Pseudo first order rate constant determined for the 60 min of reaction

VITA

Miss Malin Mungmart was born on January 3, 1981 in Bangkok, Thailand. She received the Bachelor Degree of Chemical Engineering from Faculty of Engineering, King Mongkut's Institute of Technology Ladkrabang (KMITL), in 2004. She continued her Master's study at Chulalongkorn University in June 2004.